博士論文番号：01810

Structural basis for autoinhibition and its relief of MOB1 in the Hippo pathway

(Hippo シグナル伝達経路における MOB1 の自己阻害と解除の構造基盤)

金　善龍

奈良先端科学技術大学院大学

バイオサイエンス研究科　構造生物学講座

（箱嶋　敏雄　教授）

平成 29 年 2 月 9 日提

Graduate School of Biological Sciences Doctoral Thesis Abstract

Lab name (Supervisor)	構造生物学（箱嶋　敏雄 教授）		
Name (surname) (given name)	金　善龍	Date	(2017/3/3)
Title	Structural basis for autoinhibition and its relief of MOB1 in the Hippo pathway (Hippo シグナル伝達経路における MOB1 の自己阻害と解除の構造基盤)		

Abstract

Hippo signal transduction pathway that has been delineated in *Drosophila melanogaster* as known to be a cell proliferation regulatory mechanism. Upstream regulators Merlin/Expanded activate Hippo/Salvador complex following by auto-phosphorylation of Hippo which phosphorylates Mats/Warts complex. Activated Warts kinase phosphorylates a transcriptional co-activator Yorkie; this blocks the transportation of cytoplasmic Yorkie into nucleus. In addition to this canonical pathway, several reports delineated that mammalian cells have more regulatory side branches for the Hippo pathway. Although mammalian cells have such divergent mechanisms for regulation of the upstream Hippo pathway, the results have agreed that MOB1 (Mps One binder 1, the mammalian Mats orthologue) is indispensable for LATS1/2 (Large tumor suppressor 1/2, the mammalian Warts orthologue) activation. Interactions of MOB1 and the NTR (N-terminal regulatory) domain of LATS found in front of the kinase domain of all NDR/LATS family have been reported to be essential for kinase activity. Several studies have reported that phosphorylation of Thr12 and Thr35 of MOB1 is essential for interacting with LATS/NDR kinases. However, the precise mechanisms of the MOB1 autoinhibition and its release by phosphorylation are unknown. One of difficulties in experiments for elucidating the precise mechanism was recognized that preparation of the autoinhibited full-length MOB1 protein sample was difficult because of degradation during purification.

I have successfully purified the full-length mouse MOB1B protein and determined the three-dimensional structure at 2.2Å resolution. The overall structure of MOB1B is globular shape, composed of 9 α-helices and two small fragments of β-sheet. The obtained structure of full-length MOB1B displays the well-presented core body and additional β-strand (S_N strand) and one of α-helix (Switch helix) in its N-terminal extension from the core body.

I have also determined the crystal structure of the complex between the MOB1B core domain and the LATS1 NTR domain. The NTR domain adopts a V-shape antiparallel α-helical fold and binds the site of MOB1 with both polar and nonpolar contacts. Superposition of above two MOB1 structures implies the full-length mouse MOB1B structure is the autoinhibition form, which has Switch helix of the N-terminal extension bound to the LATS1 binding site formed by the negatively-charged and nonpolar-patched molecular surfaces consisting of H1, H2 and H7 helices and H4-H5 loop. Phosphorylation of Thr35 of Switch helix structurally accelerates its dissociation from the binding site, thus enabling LATS1 binding. Moreover, I have determined the crystal structure of the complex between the MOB1B core domain and the phospho-mimic LATS1 NTR domain that have T12D and T35D mutations and showed that phosphorylated Thr12 could induce the pull-the-string mechanism by which the N-extension is uncovered from the LATS-binding site of the MOB1 core domain.

In addition, I have also determined the complex structure between the MOB1B core domain and a phosphorylated Sav1 peptide, which reveals phosphorylated residue Ser36 of Sav1 binds into the basic cluster pocket composed of residues Lys153, Arg154, and Arg157 of MOB1. This complex structure may give us a hint for understanding of the MOB1 membrane targeting mechanism.

These findings provide a physical basis for understanding the crucial roles of MOB1 in the Hippo pathway, and a clue for the future development of inhibitor or activator compounds useful in the treatment of cancer by controlling the Hippo pathway.

Content

Introduction

Division of cells should be controlled precisely, which decides the organ size during development. Loss of its control leads to tissue overgrowth or tumorigenesis. Up to this day, plenty of studies have elucidated the relationship of a number of proteins and their binding partners as key components of specific metabolic pathways which control the coordination between cell proliferation, morphogenesis and apoptosis. Members of the NDR (Nuclear Dbf2-Related) protein-kinase family, a subclass of AGC-type protein kinases, are known as the essential components of those pathways in yeasts and higher eukaryotes[1-6, 16] (**Fig. 1**).

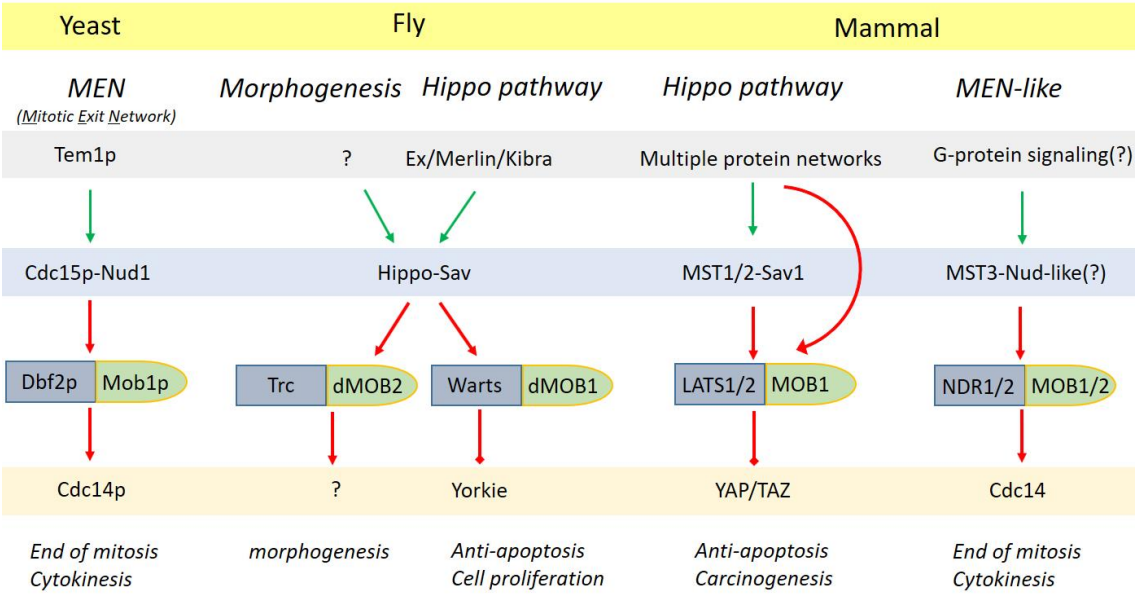

Figure 1. The schematic diagram of NDR kinase signaling pathways.
NDR kinase members are in blue boxes. Green arrows represent the positive regulation without phosphorylation. The activation by phosphorylation is depicted with red arrows.

The studies in this field have revealed on the mechanisms that base on the regulation and function of the NDR proteins by means of the co-activator MOB (Mps1-One Binder) proteins. Researches from yeast, and higher eukaryotes have highlighted the conserved and important roles of MOB proteins in the activation of NDR kinases[1-6, 16, 55]. MOB proteins play a crucial role in cell cycle regulation by interacting with and activating the NDR kinases. This subfamily of serine/threonine kinases includes Dbf2, Dbf20 and Cbk1 in *Saccharomyces cerevisiae*, Warts and Trc in *Drosophila melanogaster*, NDR1/2 and LATS1/2 (Large Tumor Suppressor 1 and 2) in human. These protein kinases share a role of regulation cell growth, division and morphology like their interacting partner MOB proteins[16, 55, 56].

As a member of NDR signal transduction pathway family, the Hippo pathway is a key signaling cascade that ensures organ size and normal tissue growth by coordinating cell proliferation and differentiation, and has now been recognized as an essential tumor suppressor cascade[1-6] (**Fig. 2**). In mammals, the core pathway components comprise two kinds of kinases, mammalian Ste20-like 1 and 2 (MST1/2) and AGC Ser/Thr protein kinase LATS1/2, in addition to transcriptional co-activator Yes-associated protein (YAP) and transcriptional co-activator with PDZ-binding motif (TAZ). To exert full kinase activity, MST1/2 and LATS1/2 requires coactivators, the scaffolding proteins Salvador homolog 1 (Sav1) and MOB1, respectively. MOB1 is mostly localized in the cytoplasm at the basal levels; however, in the active state of the Hippo pathway, Sav1-bound MST1/2 kinases phosphorylate the C-terminal hydrophobic motif of LATS1/2 and the N-terminal region of MOB1 proteins at the juxtamembrane region. Phosphorylated MOB1 protein is switched ON to increase the binding affinity to LATS1/2 and this binding accelerates auto-phosphorylation of the activation loop, A-loop (also referred to

as activation segment or T-loop)[7], of LATS1/2 kinases for full activation. Activated MOB1-bound LATS1/2 phosphorylates YAP to block its nuclear import and results in inhibition of its transcriptional programs.

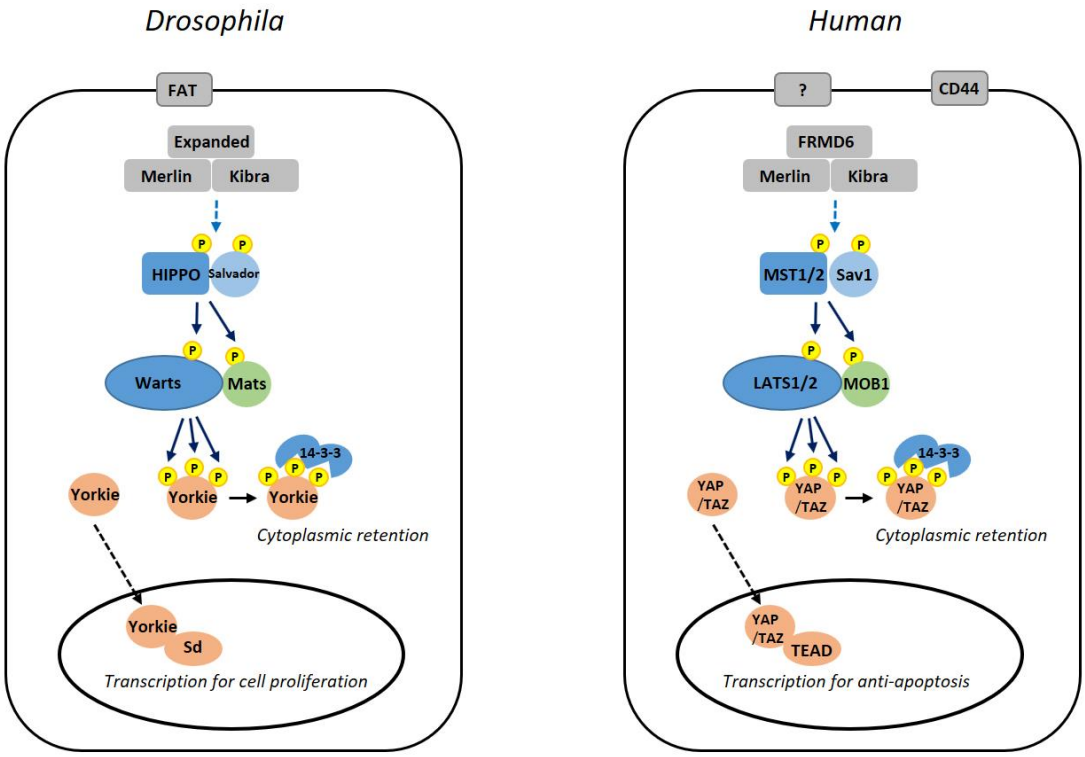

Figure 2. Schematic representations of the canonical Hippo pathway of fly and human cell.

In addition to this canonical pathway, mammalian cells possess a number of regulatory side branches for the Hippo pathway[8-12] (**Fig. 3**), whereas MOB1 is indispensable for LATS1/2 kinase activation, as shown in yeast and *Drosophila*[13-15]. As mentioned above, the importance of MOBs in protein kinase activation was also exemplified by yeast NDR1/2 kinases in the regulation of the mitotic exit network (MEN)[16] and Ace2p activity and cellular morphogenesis (RAM)[17-18](**Fig. 1**). Thus, MOB proteins act as a pivotal molecular switch both in the Hippo and MEN/RAM

pathways.

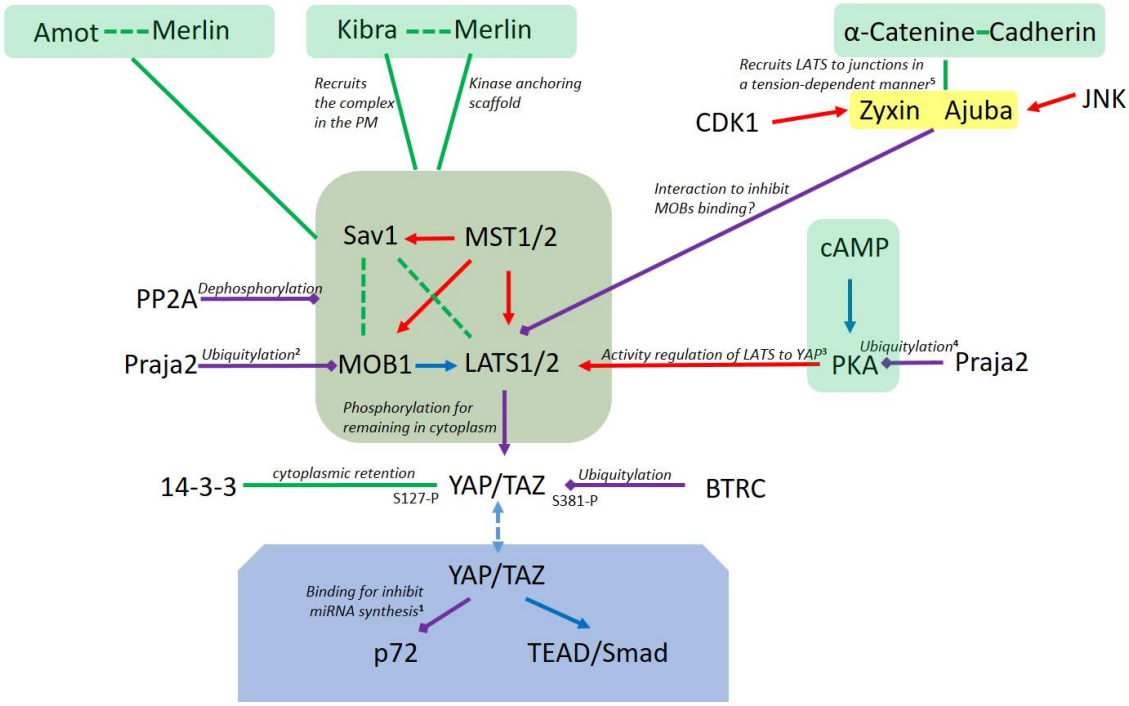

Figure 3. The regulatory side branches of Hippo pathway in mammalian cell.

In addition of the canonical pathway, mammalian cells possess a number of regulatory side branches. LIM domain protein Ajuba and Zyxin interact with LATS1/2 for inhibiting MOB1 binding. The ubiquitination also engaged in regulation of Hippo pathway. E3 ubiquitin ligase Praja2 and BTRC ubiquitylate MOB1 and YAP each other. Red arrows represent phosphorylation for the Hippo ON, Blue arrows show positive regulation without phosphorylation. Purple arrows show the regulation for Hippo OFF.

In mammals, at least six different MOB proteins are encoded by independent genes, and two closely-related (95% amino acids sequence identity) members, MOB1A and MOB1B, play redundant biological roles as co-activators of LATS1/2 and NDR1/2 kinases (LATS/NDR kinases)[15,19,20]. The phosphorylation of MOB1 occurs at two threonine residues, Thr12 and Thr35, located at the N-terminal extension out of the

C-terminal globular MOB core domain (**Fig. 4**), and is required for binding to LATS/NDR kinases[19-20].

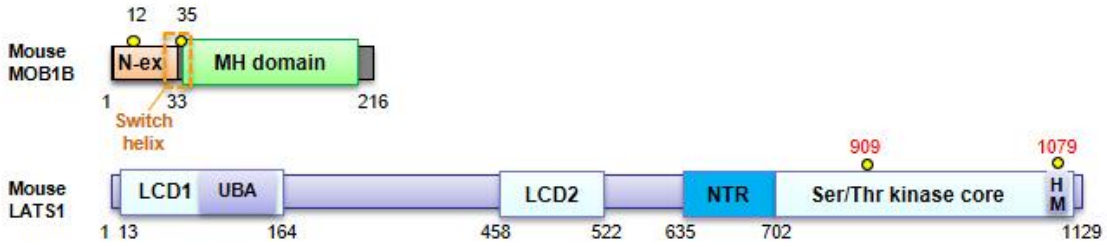

Figure 4. A schematic representation of domain organization and the phosphorylated residues of MOB1B and LATS1

Unfortunately, the N-terminal extension of MOB1 is easily degraded during protein purification and all reported MOB1 structures have been based on N-terminal truncated forms[21-25]. Lack of a full-length MOB1 structure in the autoinhibited form is hampering efforts to fully understand the mechanism by which Thr12/Thr35-phosphorylation activates MOB1. Insights into this area are crucial, since the phosphorylation of human MOB1 appears to be important in cell proliferation and the suppression of carcinoma development[19,26]. Biochemical evidence suggests that phosphorylated MOB1 binds the highly conserved N-terminal regulatory (NTR) region of LATS/NDR kinases[27-32]. The NTR region is located at the immediate front of the catalytic domain (**Fig. 4**) and is essential for kinase activity[19,16,32]. Recently, two X-ray structures of MOB1 bound to LATS/NDR kinases have been reported: one is a low resolution (3.3 Å–4.5 Å) structure of yeast truncated Mob2p bound to the NDR-like kinase Cbk1p in the RAM pathway, the Mob2p-Cbk1p complex[33] and the other structure is that of human phosphorylated MOB1A bound to the NTR domain of LATS1, the pMOB1A-LATS1 structure[34].

However, I found that the structures of the NTR domains and their binding modes in these recently-reported complexes display sharp discrepancies, which should be solved by additional experiments.

Here, I report the results of structural and biochemical studies of full-length mouse MOB1B in the autoinhibited form and those of the MOB core domain bound to the NTR region of LATS1 (hereafter referred to as the MOB1B-LATS1 complex). The structure of full-length MOB1B reveals that the N-terminal extension comprising a positively-charged region followed by Switch α-helix binds directly to the LATS1-binding surface to block LATS1 binding and this blocking is stabilized by β-sheet formation between S_N strand of the N-terminal extension and S2 strand of the core domain. The full-length MOB1B structure suggests that phosphorylation of Thr12/Thr35 causes relief of autoinhibition by inducing destabilization of Switch helix binding to the LATS1-binding site. This autoinhibited mechanism differs from the recently-proposed model in which the N-terminal $FxFx_5KxF$ motif occupies part of the LATS1-binding surface[34]. The autoinhibited form of full-length MOB1B suggests that N-terminal truncated MOB1B should be capable of binding LATS1. I confirmed this hypothesis by determining the complex structure between N-terminal truncated MOB1B and the NTR domain of LATS1, the MOB1B-LATS1 complex. I found that MOB1B-LATS1 complex structure is essentially the same as the recently reported complex structure between phosphorylated MOB1A and the NTR domain of LATS1, the pMOB1A-LATS1 complex[34], which established the bihelical V-shaped structure of the NTR domain and its specific interactions with conserved residues located at the LATS1-binding surface. However, the binding mode found in these complex structures differs from that described for the recently-reported structures of the yeast

Mob2p-Cbk1p complexes[33]. The MOB1B-LATS1 and pMOB1A-LATS1 structures are consistent with my mutational data and relevant experimental data from the literature, in contrast to those of the Mob2p-Cbk1p complexes. I have concluded that the structural discrepancy is not due simply to intrinsic differences between mouse/human MOB1B and yeast Mob2p.

Despite the core regulatory mechanism which is the phosphorylation cascade from MST1/2 to YAP/TAZ of the Hippo pathway has been delineated with the intensive efforts, the upstream regulation mechanism is still to be studied. MOB1 is generally regarded as the cytoplasmic protein. However, several evidences show that MOB1 should be transported to the plasma membrane, then phosphorylated by MST1/2 for activating LATS1/2[30, 52]. By simple MOB1 overexpression, LATS1/2 cannot be activated even though they have high affinity[28]. Membrane targeted Mats (*Drosophila* MOB1) goes so far as to be able to inhibit tissue growth in the absence of Hpo (*Drosophila* MST1/2)[52]. Although this subcellular localization of MOB1 at the plasma membrane is essential for LATS1/2 activation, the precise membrane targeting mechanism is to be delineated. In this thesis, I also show the complex structure of MOB1B and phosphorylated Sav1 peptide, which suggests a model of the subcellular localization mechanism of MOB1 in the Hippo pathway.

These studies enhance our understanding of the molecular mechanisms involved in the regulation of the Hippo pathway and provides a clue for the future developments of tissue repair or anticancer drug strategies.

Results

The overall structure of full length MOB1B.

As reported previously for human and *Xenopus* MOB1[21-22], the N-terminal extension of mouse MOB1B was also protease sensitive. However, I successfully purified full-length MOB1B by low-temperature expression (see experimental procedures) and quick purification without degradation (**Fig. 5**), and determined the three-dimensional structure at 2.2Å resolution (**Fig. 6**) (**Table 1**). The asymmetric unit contains four independent molecules (**Fig. 6a**), which display no large conformational changes (**Fig. 6b**). The overall structure adopts a globular shape comprising the MOB core domain made of nine α-helices (H1-H9) with the N-terminal extension, which forms a β-strand (the S_N strand, residues 5-9) at the N-terminal segment of FLFGSRSS (residues 3-10) and a newly formed 4-turn α-helix (residues 24-38, hereafter referred to as the Switch helix), whereas the 10-residue linker between the S_N strand and the Switch helix were poorly defined on the current map. Notablly, the S_N strand forms a β-sheet with the S2 strand (residues 95-98) (**Fig. 8b**).

The MOB core domain is composed of nine α-helices H1-H9 and two small β-strands (S1 and S2), which form a hairpin-like structure (**Fig. 7** and **Fig. 8a**). The nomenclature employed for secondary structures follows that utilized for the first MOB1 structure, human MOB1A[21]. One zinc ion is coordinated by two cysteine (Cys79 and Cys84) and two histidine (His161 and His166) residues (**Fig. 6c**) and linked to the H3-S1 loop and the C-terminal part of the H5 helix as found in the structures of other MOB proteins[21, 25] (**Fig. 8b**). Thus, the core domain of MOB1B displays essentially the

same structure as those of the N-terminal truncated free forms of human MOB1A[21], *Xenopus* MOB1[22], and yeast Mob1p[23] (**Fig. 8c**).

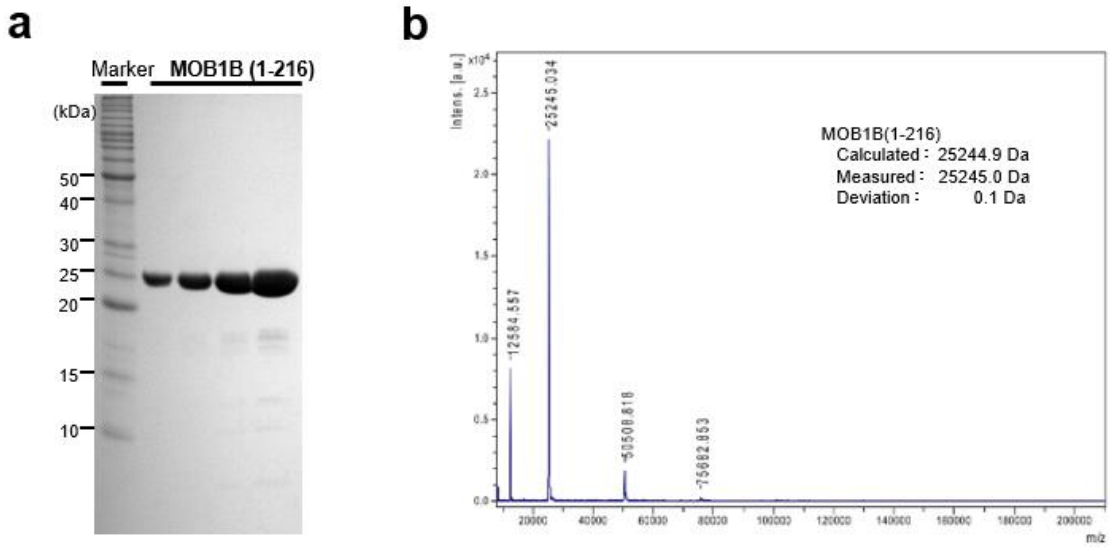

Figure 5. Full length MOB1B was purified without degradation.

(**a**) SDS-PAGE of the purified full-length MOB1B. The purified sample gave a single band corresponding to ~25 kDa mass.

(**b**) MALDI TOF MS spectrum of the purified full-length MOB1B. The spectrum confirmed that the protein had been successfully purified without degradation.

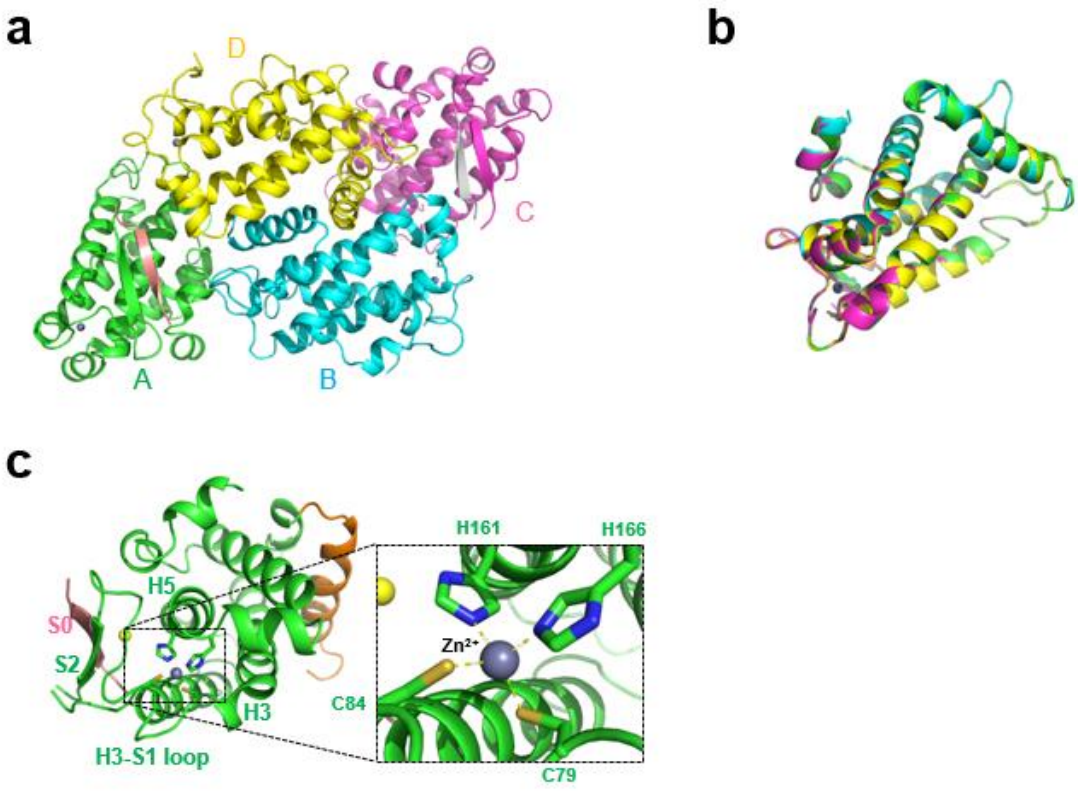

Figure 6. Structures of the zinc-, peptide- and chlorine ion-binding sites of full-length MOB1B. (**a**) Crystal packing of full-length MOB1B. Four crystallographically-independent molecules in the asymmetric unit of the crystal are shown in different colors, molecules A (green), B (cyan) C (magenta) and D (yellow). In molecules A and D, S2 strand bind S0 to form an antiparallel β-sheet. (**b**) Overlay of four crystallographically-independent molecules in the asymmetric unit of the crystal. No significant deviations were found with a small averaged r.m.s. deviation (0.26 Å). (**c**) The zinc ion-binding site of full-length MOB1B. The zinc ion was coordinated with His61 and His66 from H3-S1 loop, and Cys79 and Cys84 from H5 helix.

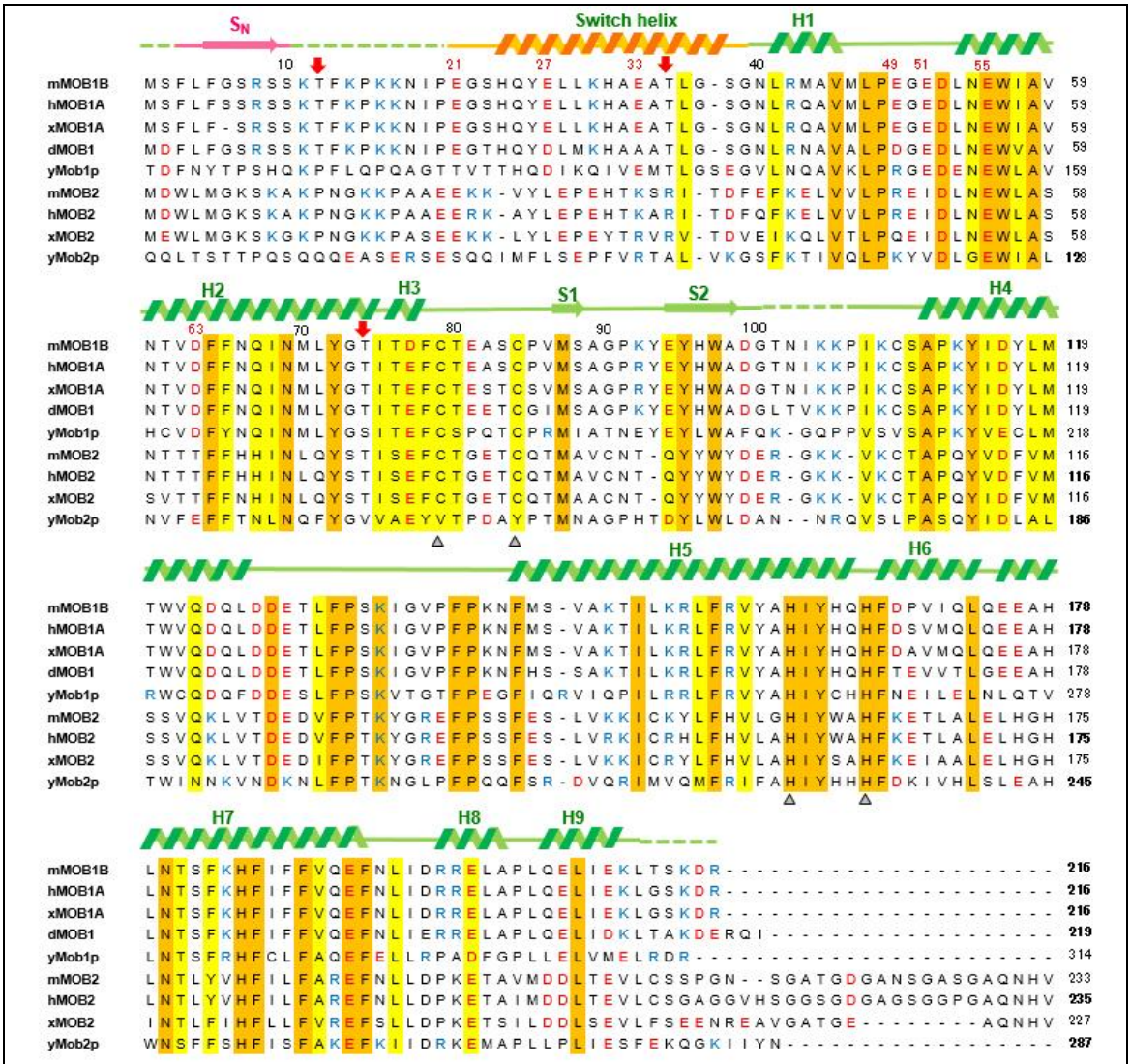

Figure 7. Sequence alignment of MOB proteins and the secondary structure elements found in the full-length MOB1B structure of the current study.

The secondary structure elements found in MOB1B structures are shown at the top with α-helices (springs, H1-H9) and β-strands (arrows, S0-S2). In the structure, S1 strand (Met87-Ser88-Ala89) is deformed but forms a type-I β-hairpin with S2 strand as in the structure of the N-terminal truncated human MOB1A ([21] Stavridi *et al*., 2003). MOB sequences are from mouse (m), human (h), *Xenopus* (x), *Drosophila* (d) and yeast (y). Three threonine residues of mouse MOB1B, Thr12, Thr35 and Thr74, are marked with red arrows at the top. Two cysteine and two histidine residues (Cys79, Cys84, His161 and His166 of mouse MOB1B) are marked with grey arrow heads at the bottom. Acidic and basic residues are shown in red and blue, respectively. Conserved residues are highlighted in orange and semi-conserved in yellow. Acidic residues interacting with LATS1 are numbered at the top.

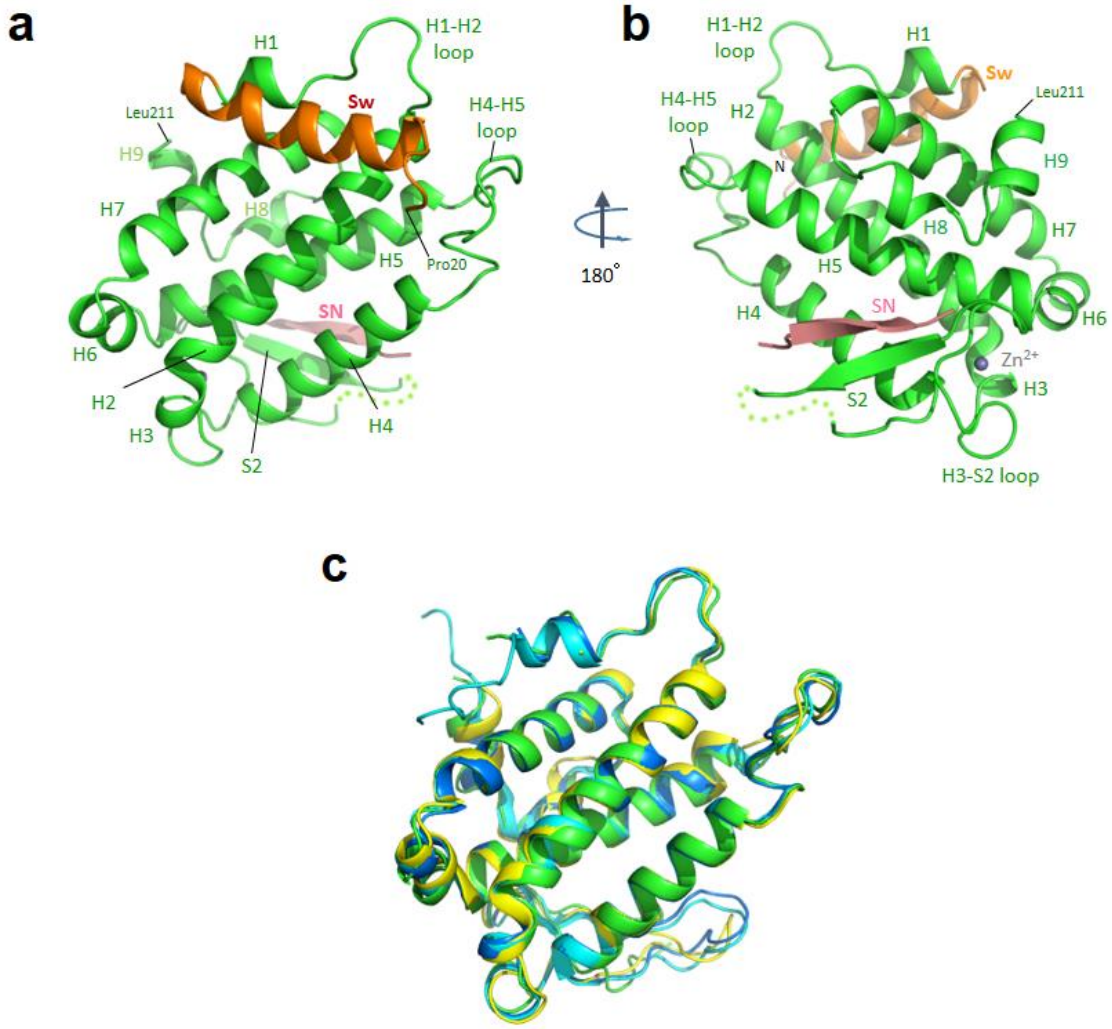

Figure 8. The full-length MOB1B structure shows the autoinhibited form of MOB1.

(**a**) The structure of full-length MOB1B in this study. The front view of MOB1B showing Switch helix (Sw in orange) bound to α-helices (H1, H2, and H7) and H4-H5 loop. S_N strand (in pink) forms a β-sheet with S2 strand. On the current electron density map, five residues (101-105, indicaed by a dotted line) in S2-H4 loop were not modeled because of poor density. The nomenclature of secondary structures is followed by that in the first MOB1 structure, human MOB1A ([21] Stavridi *et al.*, 2003).

(**b**) As in **b**, but rotated around the vertical axis to show the backside of the molecule. A zinc ion (a gray ball) is located at a space between H3-S1 loop and H5 helix.

(**c**) Structural comparison of full-length mouse MOB1B and the related MOB structures. The MOB core domain of full-length mouse MOB1B (green) was superimposed with human MOB1A (cyan), yeast Mob1p (yellow) and phosphopeptide-bound human MOB1A (blue). Each root mean squares (r.m.s.) deviation on overlay with mouse MOB1B is 0.9 Å (human MOB1A), 2.1 Å (*Xenopus* MOB1) and 1.2 Å (yeast Mob1p).

MOB1B exists as a monomer in solution

The analytical ultracentrifugation (AUC) experiments of full-length MOB1B, its phosphomimic (T12D/T35D) double-mutant and the N-terminal 32-residue truncated form show a single monomeric peak at ~30 kDa, indicating that MOB1B exits as a monomer in solution (**Fig. 9**). Yeast Mob1p, however, was proposed to form a dimer in solution, based on the light-scattering data and crystal packing showing part of its N-terminal residues making intermolecular contacts with an asymmetric mate[23]. This discrepancy could be attributed to absence of the extremely long N-terminal extension (~140 residues) of yeast Mob1p. The helical region (H0, residues 126-139) of yeast Mob1p partially overlaps with the Switch helix, although the sequence homology is poor (**Fig. 7**). Another reason for the discrepancy may be the higher protein concentration (~20 mg/ml, ~700 μM) utilized in the light-scattering experiments compared to that employed in my experiments (19 μM). I confirmed a monomer in a higher concentration (200 μM) of full-length MOB1B (**Fig. 9**) and thus concluded that MOB1B exists as a monomer in solution.

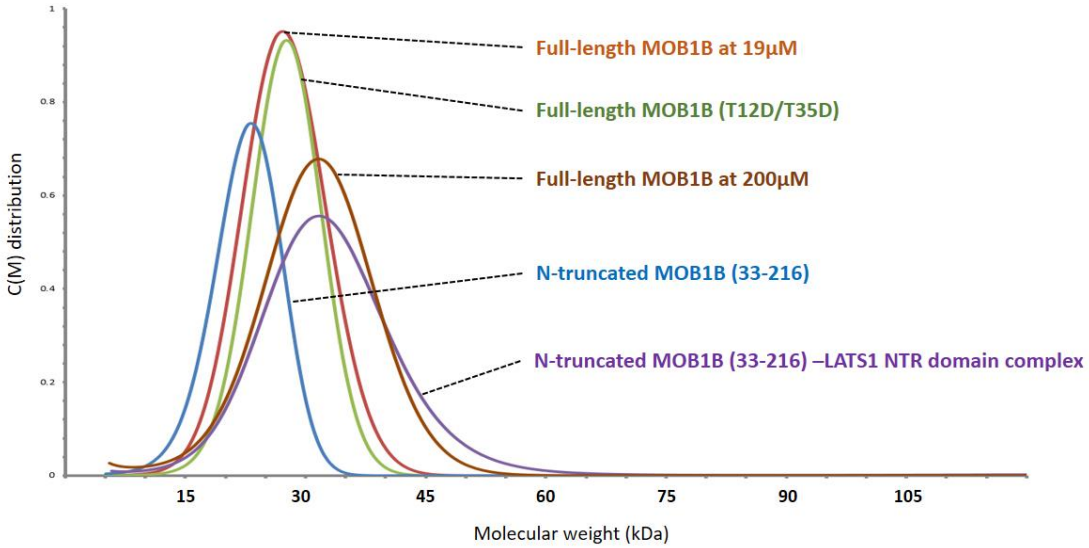

Figure 9. Ultracentrifugal analysis reveals MOB1B exists as a monomer in solution.
The sedimentation velocity ultracentrifugation analyses of full-length, N-terminal 32-residue truncated, and mutant (T12D/T35D) MOB1B show all these molecules exist as a monomer in solution. All samples contain 19μM protein, other than the high-concentration (200 μM) of full-length MOB1B. The calculated molecular mass of each sample is 26.9 kDa for full-length MOB1B (19 μM), 27.2 kDa for mutant full-length MOB1B (T12D/35D), 22.2 kDa for N-terminal truncated MOB1B, 31.8 kDa for the N-terminal truncated MOB1B-LATS1 complex, and 30.6 kDa for 200 μM full-length MOB1B.

Table 1. Crystallographic and refinement statistics of full-length MOB1B [a].

Data collection		**Refinement**	
Space group	$P2_1$	No. atoms	
Cell parameters [Å]	a =59.36, b = 127.69, c = 59.30	Protein	6,323
V_M [Å^3/Da] / V_{sol} [%]	2.22 / 44.71	Zn^{2+} ion	4
SPring-8 beam line	BL44XU	Cl^- ion	2
Resolution [Å] [b]	30-2.20 (2.24-2.20)	Solvent	153
Wavelength [Å]	0.9000	R_{work} / R_{free} [%] [c]	23.3 /24.6
Reflections (unique)	159,366 (44,345)	Ramachandran plot	
Completeness [%]	99.3 (100)	Favored [%]	96.4
Redundancy	3.6 (3.8)	Allowed [%]	3.6
Mean I/σ_I	37.7 (3.5)	Outliers [%]	0
R_{merge} [%]	6.3 (55.4)	r. m. s. deviations	
		Bond lengths [Å]	0.013
		Bond angles [°]	1.323
		Average B-factor [Å^2]	
		Protein	58.8
		Zn^{2+} ion	60.0
		Cl^- ion	69.7
		Solvent	57.6

Table 2. Crystallographic and refinement statistics of MOB1B-LATS1 complex [a].

Data collection		**Refinement**	
Space group	$C2_1$	No. atoms	
Cell parameters [Å]	a =78.75, b = 71.76, c = 57.86	Protein	1420/546 (MOB1/LATS1)
V_M [Å^3/Da] / V_{sol} [%]	2.29 / 46.39	Zn^{2+} ion	1
SPring-8 beam line	BL41XU	Cl^- ion	-
Resolution [Å] [b]	30-2.96 (3.00-2.96)	Solvent	-
Wavelength [Å]	1.0000	R_{work} / R_{free} [%] [c]	23.4 /27.0
Reflections (unique)	19,931 (6,660)	Ramachandran plot	
Completeness [%]	94.1(82.5)	Favored [%]	92.6
Redundancy	3.2 (3.1)	Allowed [%]	6.5
Mean I/σ_I	21.4 (2.3)	Outliers [%]	0.9
R_{merge} [%]	7.4 (56.5)	r. m. s. deviations	
		Bond lengths [Å]	0.003
		Bond angles [°]	0.745
		Average B-factor [Å^2]	
		Protein	103.0/98.9
		Zn^{2+} ion	107.4
		Cl^- ion	-
		Solvent	-

Table 3. Crystallographic and refinement statistics of MOB1B(T12/35D)-LATS1 [a].

Data collection		**Refinement**	
Space group	$C222_1$	No. atoms	
Cell parameters [Å]	a =168.7, b = 301.44, c = 127.4	Protein	11,855/4,750 (MOB1/LATS1)
V_M [Å^3/Da] / V_{sol} [%]	2.84 / 56.71	Zn^{2+} ion	8
SPring-8 beam line	BL44XU	Cl^- ion	7
Resolution [Å] [b]	30-3.55 (3.61-3.55)	Solvent	-
Wavelength [Å]	0.9000	R_{work} / R_{free} [%] [c]	21.6 /26.2
Reflections (unique)	297,262(39,931)	Ramachandran plot	
Completeness [%]	100 (100)	Favored [%]	95.7
Redundancy	7.5 (7.6)	Allowed [%]	3.3
Mean I/σ_I	21.0 (3.8)	Outliers [%]	1
R_{merge} [%]	15.3 (72.4)	r. m. s. deviations	
		Bond lengths [Å]	0.003
		Bond angles [°]	0.754
		Average B-factor [Å^2]	
		Protein	101.9
		Zn^{2+} ion	135.8
		Cl^- ion	57.1
		Solvent	-

Table 4. Crystallographic and refinement statistics of MOB1B-pSav1 complex [a].

Data collection		**Refinement**	
Space group	$P2_12_12_1$	No. atoms	
Cell parameters [Å]	a = b = 52.94, c = 59.30	Protein	2,932/191 (MOB1/Sav1)
V_M [Å^3/Da] / V_{sol} [%]	1.78 / 31.02	Zn^{2+} ion	1
SPring-8 beam line	BL44XU	Cl^- ion	-
Resolution [Å] [b]	50-1.45 (1.48-1.45)	Solvent	197
Wavelength [Å]	0.9000	R_{work} / R_{free} [%] [c]	12.5 /16.0
Reflections (unique)	279,805 (35,759)	Ramachandran plot	
Completeness [%]	98.0 (97.7)	Favored [%]	98.9
Redundancy	8.0 (8.1)	Allowed [%]	1.1
Mean I/σ_I	50.4 (4.6)	Outliers [%]	0
R_{merge} [%]	6.3 (76.0)	r. m. s. deviations	
		Bond lengths [Å]	0.022
		Bond angles [°]	1.939
		Average B-factor [Å^2]	
		Protein	27.9
		Zn^{2+} ion	18.8
		Cl^- ion	-
		Solvent	42.3

[a] One crystal was used for each data set. The total oscillation range was 180°.

[b] Numbers in parentheses refer to statistics for the outer resolution shell.

[c] $R_{work} = \Sigma | \ | F_{obs} \ | - | F_{calc} \ | \ | / \Sigma | F_{obs} \ |$. R_{free} is the same as R_{work} except that a 5% subset of all reflections was held aside throughout the refinement.

Switch helix formation and binding to the MOB core domain.

The Switch helix is stabilized by forming N-terminal capping with Ser23 and intra-helical salt bridges (Glu27-His31 and Lys30-Glu33) at the helix surface (**Fig. 10a**). The Switch helix is connected to a Gly-Ser-Gly (37-39) linker, which may be conformationally flexible and responsible for the observed protease susceptibility[21-23, 25], followed by the H1 helix and stabilized by the N-terminal cap of Asn40. The Switch helix-binding site on the MOB core domain is formed by helices H1, H2 and H7 and the H4-H5 loop, and is characterized by a conserved cluster of negative charges with nonpolar patches (**Fig. 10b**). This site is overlapped with the LATS1 binding surface found in the structures of the pMOB1A-LATS1 complex[34], the Mob2p-Cbk1p complex[33] and the MOB1B-LATS1 complex, which are described below in detail, suggesting that the autoinhibition is caused by Switch helix binding, which structurally blocks LATS/NDR binding. This molecular surface corresponds to that previously hypothesized to interact with LATS/NDR kinases[21-22].

The interface between the Switch helix and MOB core domain contains several polar and nonpolar contacts. Positively-charged His24 forms salt bridges with Glu51 and Glu55 and bifurcated hydrogen bonds to Glu51 to lock the Switch helix onto the MOB core domain (**Fig. 10a**). Nonpolar residues (Leu28, Leu29, Ala32, and Leu36) of the Switch helix contact the nonpolar patches formed by the H1 helix (Leu41), H2 helix (Trp56, Val59) and H4-H5 loop (Ile136). The phosphorylation residue of Switch helix (Thr35) is located at the edge of the interface with the MOB core domain and forms two hydrogen bonds to the helix main chains (**Fig. 10a**). Therefore, once phosphorylation occurs, phosphorylated Thr35 structurally inhibits binding of the Switch helix to the MOB core domain, which is consistent with previous reports that showed a critical role

of Thr35 phosphorylation in LATS2 activation[20]. The structure also implies that the active site of MST1/2 kinases could not access the side chain of Thr35 without dissociation of the Switch helix from the core domain, suggesting that MST1/2 traps the transiently dissociated Switch helix, the latter involved in a dynamic association-dissociation process.

Peptide-binding site formed by a β-sheet

The N-terminal S_N strand forms an antiparallel β-sheet with the S2 strand, which is located at the molecular surface opposite the Switch helix (**Fig. 10c**). This β-sheet formation is reminiscent of the intermolecular β-sheet formed in the complex between Nud1-like phospho-peptide and human MOB1[24]. In the full-length MOB1B structure, one chlorine anion binds the basic cluster pocket (formed by Lys153, Arg154 and Arg157 from helices H4 and H5) (**Fig. 10d**), which corresponds to the phosphate-binding pocket for the Nud1-like phospho-peptide, suggesting that the S2 strand and the basic cluster pocket provide an active site for inter- or intramolecular interactions. Meanwhile, the MOB1B and phospho-Sav1 peptide complex structure is essentially same as the complex structure of MOB1A and Nud1-like phospho-peptide (described later in detail).

Another phosphorylation residue, Thr12, is located at the conformationally flexible part of the N-terminal extension, flanking the C-terminal end of the S_N strand, indicating that this residue may be easily accessible to phosphorylation by MST1/2, and contrasts that of Thr35 which is partially buried at the interface between the Switch helix and core domain (**Fig. 10a**).

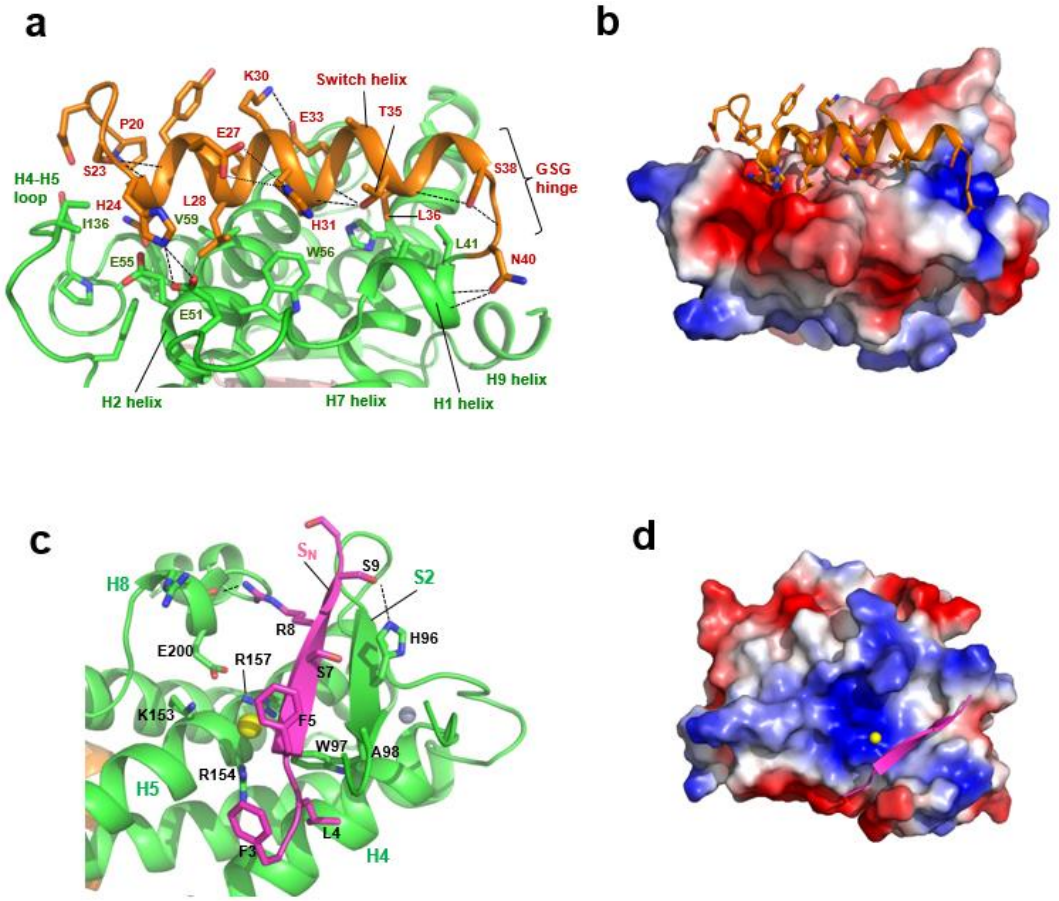

Figure 10. The N-terminal extension binds the core domain by forming S_N strand and Switch helix.

(**a**) A close-up view of Switch helix bound to the MOB core domain. Switch helix (orange) binds the MOB core domain (green). Switch helix is stabilized by intra-helical salt bridges/ionic hydrogen bonds (broken lines) and both polar and nonpolar interactions with the MOB core domain. One of the phosphorylation threonine, Thr35, exists at the interface and makes hydrogen bonds to the main-chain carbonyl groups of Ala31 and His32 of Switch helix.

(**b**) Electrostatic potential surface shows Switch helix binding to the negatively-charged (red) and nonpolar-patched molecular surface formed by α-helices H2 and H7 and H4-H5 loop (see text).

(**c**) A close-up view of the peptide-binding site of Molecule-A. S_N strand (magenta) binds the peptide-binding site by forming a β-sheet with S2 strand and being stabilized by nonpolar contacts of Leu4 with Trp97, and Phe5 with Ala98, and hydrogen bonds of Arg8 to H8 helix, and Ser7 and Ser9 with His96. The peptide binding site is adjacent to the basic cluster pocket formed by Lys153, Arg154 and Arg157 from H4 and H5 helices. The bound chlorine anion (a yellow ball) is located at

the center of the basic residues, which is the phosphate group-binding site in the structure of human MOB1 bound to the Nud1-like phospho-peptide[24].

(**d**) The electrostatic potential surface of the basic cluster pocket.

Contribution of the S_N strand to MOB1 autoinhibition

Then I set out to determine which part of the N-terminal extension is essential for MOB1 autoinhibition. To this end, a series of N-truncated MOB1B protein constructs were generated for binding assays to measure reduction in autoinhibition with deletion (**Fig. 11a**). Interestingly, truncation of the N-terminal 10 residues resulted in enhanced affinity with LATS1 NTR domain compared with that of the full-length form, suggesting that formation of the β-sheet between the S_N and S2 strands contributes to stabilization of the autoinhibited form. Truncation of the N-terminal 16 and 21 residues removes the N-terminal S_N strand and the linker, but not the Switch helix, and resulted in a large reduction in autoinhibition (**Fig. 11b**). The peptide region targeted for the truncation contains basic residues (4 Lys residues), which may contribute to the autoinhibition by electrostatically interacting with the negatively-charged LATS1-binding surface of the MOB1 core domain. These results are essentially consistent with a recent report detailing truncation of the N-terminal 15 or 32 residues[34].

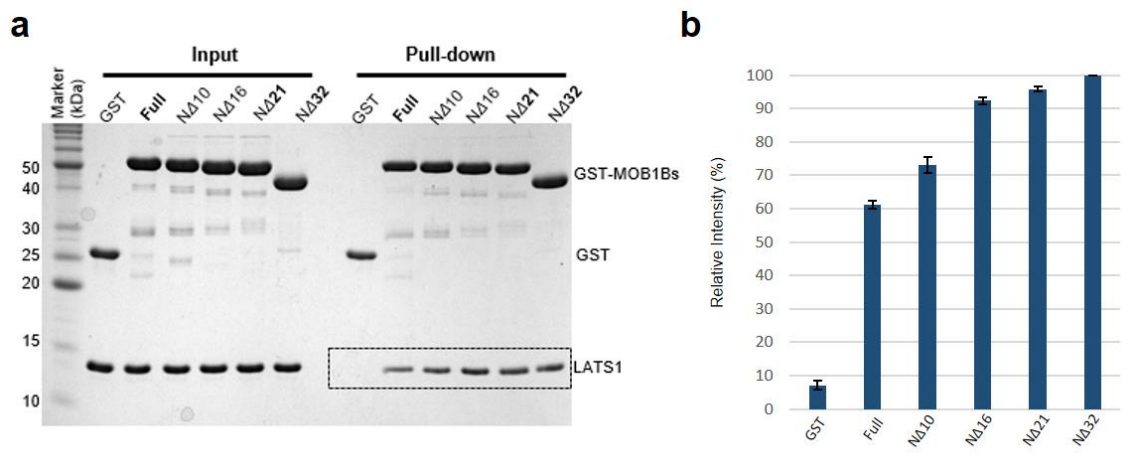

Figure 11. S_N strand of the N-terminal extension of MOB1B contributes to stabilization of the autoinhibited form.

(**a**) Pull-down binding assays of the NTR domain of LATS1 with GST-N-terminal truncated MOB1B. MOB1B proteins are the N-terminal 10, 16, 21, and 32-residue truncated forms, *Δ*10, *Δ*16, *Δ*21 and *Δ*32, respectively, with full-length form (Full). The full-length MOB1B exhibits a residual binding affinity to the NTR domain of LATS1, being in consistent with the reported weak binding of full-length MOB1A to LATS1 ([34] Ni *et al.*, 2015).

(**b**) Histogram of relative LATS1 binding (100% for GST-N-truncated *Δ*32 MOB1B) shown in **a**.

Structure of the N-truncated MOB1B-LATS1 complex

As discussed later, I found a serious discrepancy between the reported structures of the pMOB1A-LATS1 complex[34] and the Mob2p-Cbk1p complex[33]. I determined the structure of the complex between the N-truncated dominant active form of MOB1B in complex with the NTR domain of LATS1 to independently ascertain which structure of the MOB1-LATS1 complex is correct. The crystal structure of the complex between the NTR (residues 621-703) domain and N-terminal truncated MOB1B (33-216) was determined at 2.96 Å resolution (**Table 2**). The structure reveals that the NTR domain forms a V-shaped bihelical structure formed by antiparallel long helices, αA (Gln636-Met668) and αB (Gln674-Ala697), which bind the negatively-charged and nonpolar patched surface of MOB1B (**Figs. 12a-c**). The V shape of the NTR domain is stabilized by formation of an inter-helical hydrophobic core with nonpolar residues (Leu663 and Met667 from the α1 helix, Leu672 from the connected loop, and Met680 and Leu684 from the α2 helix) and inter-helical salt bridges comprising residues, Arg659-Glu688 and Glu664-Arg681 (**Figs. 13a, b**). The obtained structure is essentially the same as that of the pMOB1A-LATS1 complex[34], with small overall root mean square (r. m. s.) deviation (0.79 Å) (**Fig. 12d**). Furthermore, the complex structure between the phosphomimetic form of MOB1B bound to the LATS1 NTR domain also displays a similar structure to that of the pMOB1A-LATS1 complex (**Fig. 12e**).

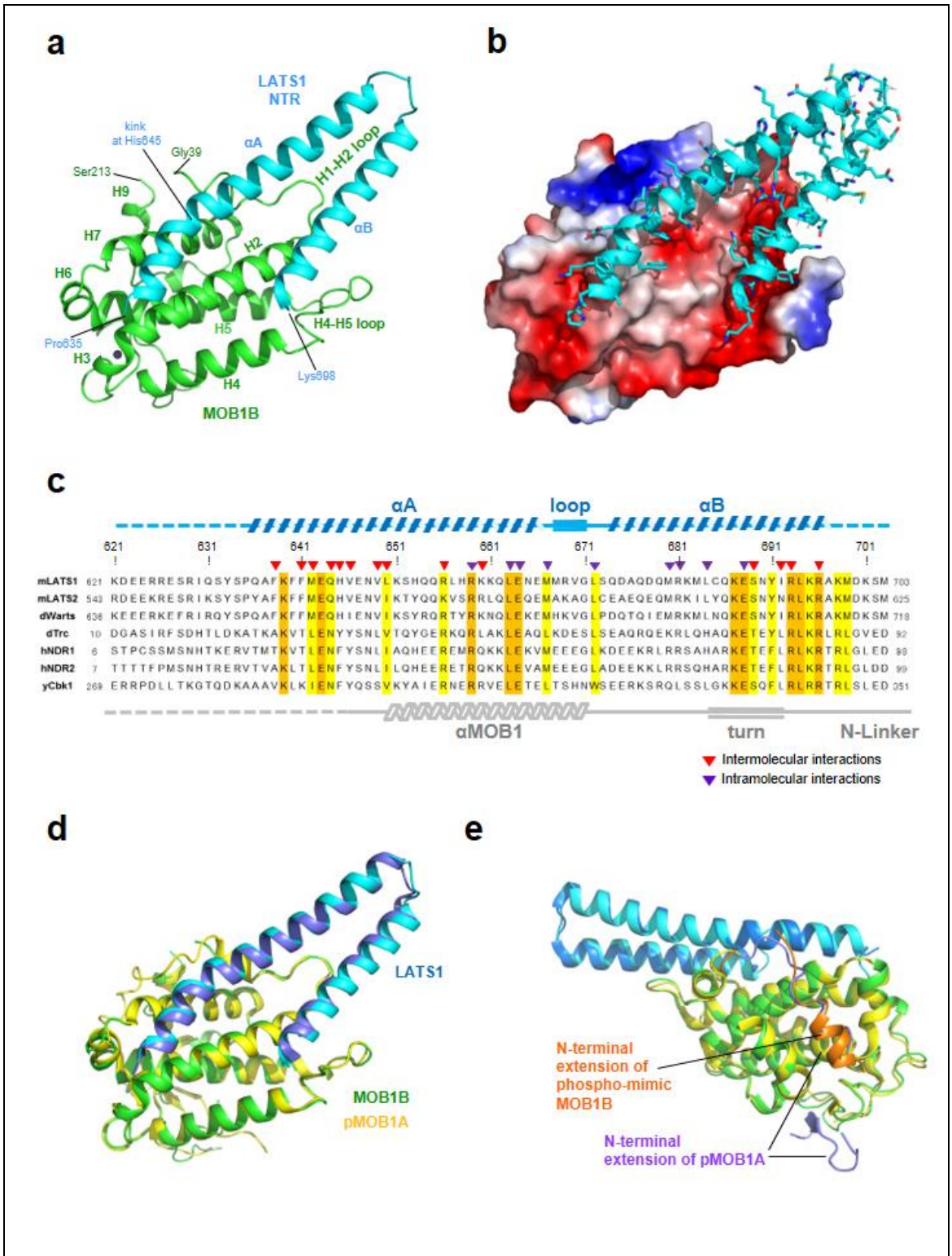

Figure 12. The structure of the MOB1B-LATS1 complex.

(**a**) The structure of the complex between the N-truncated MOB1B (residues 33-216, green) and the NTR domain (621-703, cyan) of LATS1.

(**b**) As in **a**, but MOB1B is shown as electrostatic potential surfaces and the LATS NTR domain in a

ribbon model with side chains as in stick models.

(**c**) Sequence alignment of the NTR domains of LATS and NDR kinases. The secondary structure elements of MOB1B-LATS1 complex structure are shown at the top with broken lines for residues undefined in the current electron density map. Two helices contain conserved (orange) and semi-conserved (yellow) residues. Both polar and nonpolar residues participate in intermolecular interactions (red arrow heads) with MOB1B, and intramolecular interactions (purple arrow heads) stabilizing the NTR bihelical structure. The N-terminal 14 residues and a short C-terminal segment of 5 residues are unstructured (broken lines).

(**d**) Overlay of the structure of the N-truncated MOB1B-LATS complex (MOB1B in green and the NTR domain of LATS1 in cyan) on that of the pMOB1A-LATS1 complex (5BRK).

(**e**) Overlay of the structure of the phosphomimic MOB1B-LATS complex (MOB1B in green and the NTR domain of LATS1 in cyan) on that of the pMOB1A-LATS1 complex (5BRK).

Inter- and intramolecular interactions of the MOB1B-LATS1 complex

The major intermolecular interaction between MOB1B and the NTR domain occurs primarily at the sidechain level with both nonpolar and polar contacts but also includes direct interactions involving the backbone of MOB1B (**Fig. 14**). The helical axis of the αA helix is kinked at His645 (**Fig. 12a**) with the following part of the αA helix docked into the hydrophobic groove between antiparallel helices H2 and H7, and the αB helix interacts with the negatively-charged patch (**Fig. 12b** and **Figs. 13c, d**). Four negatively-charged acidic residues (Glu49 and Glu51 from the H1-H2 loop, and Glu55 and Asp63 from the H2 helix) of MOB1B form direct salt bridge/hydrogen bond formations with six positively-charged residues (His645, Arg656, Arg659 and Lys660 from the α1 helix, and Arg693 and Arg696 from the α2 helix) from the NTR domain (**Fig. 15**).

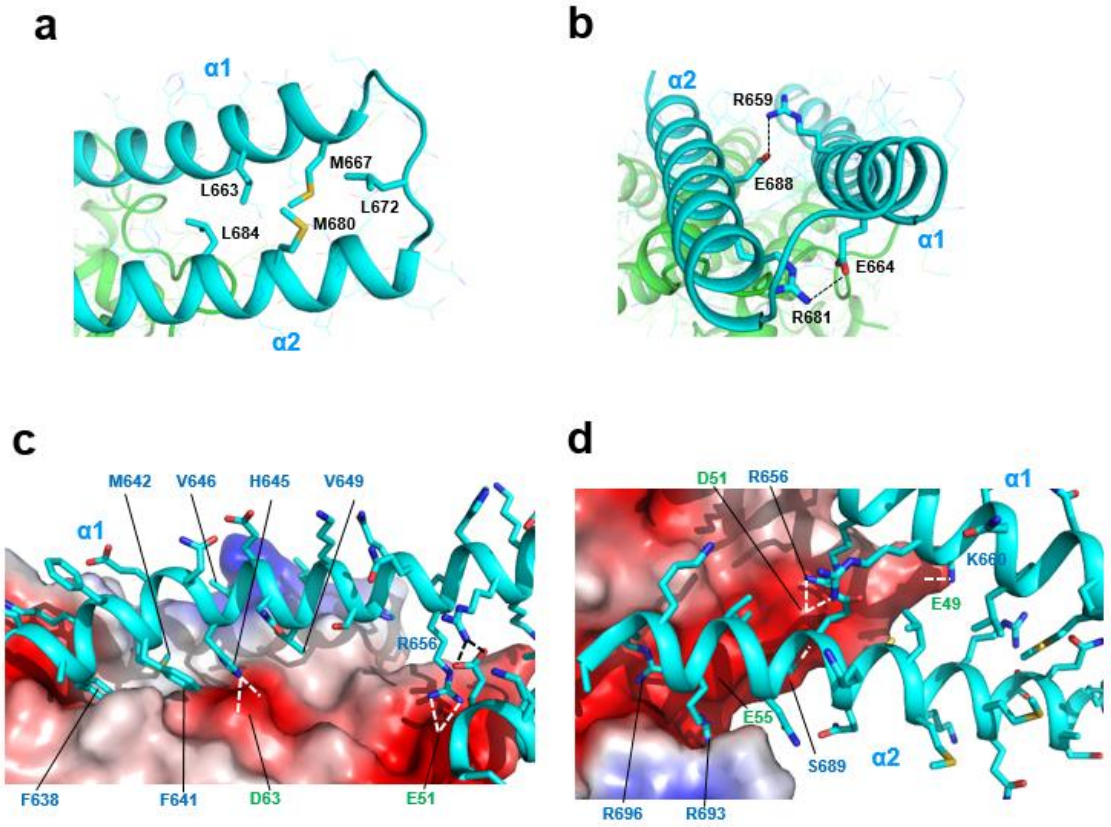

Figure 13. Inter- and intramolecular interactions stabilizing the V-shape structure of the NTR domain of LATS1.

(**a**) A close-up view of the inter-helical hydrophobic core formed by nonpolar residues from α1 helix (Leu663, Met667), the connected loop (Leu672) and α2 helix (Met680 and Leu684).

(**b**) A close-up view of inter-helical salt bridges/hydrogen bonds, Arg596-Glu688 and Glu664-Arg681.

(**c**) A close-up view of the N-terminal region of α1 helix from the NTR domain of LATS1 bound to the groove between H1 and H7 helices of MOB1B. The interactions are shown with broken lines.

(**d**) A close-up view of the helix bundle of the NTR domain of LATS1 bound to the negatively-charged groove between H1 and H7 helices of MOB1B.

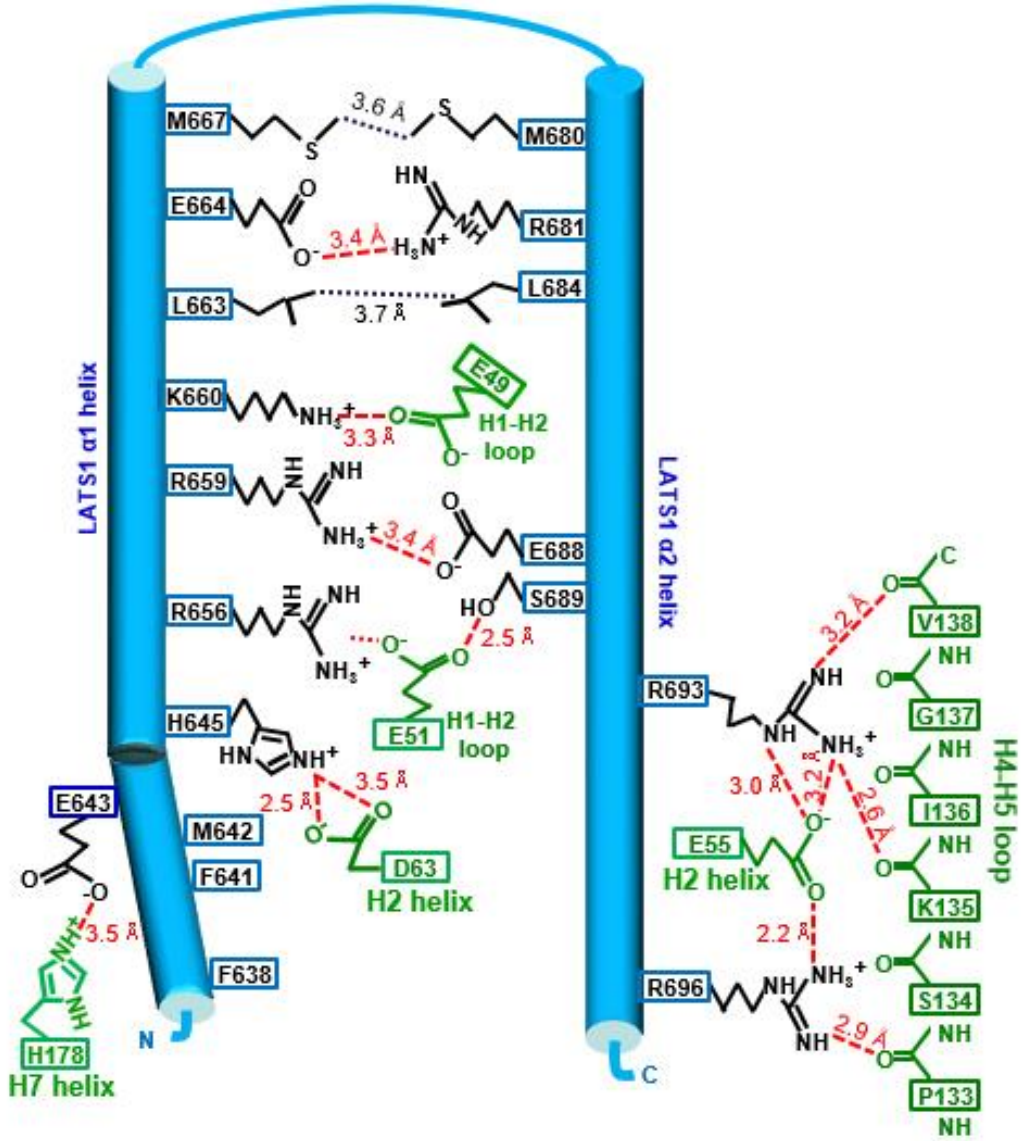

Figure 14. Summary of intermolecular salt bridges/hydrogen binds between the NTR domain of LATS1 and the core domain of MOB1B (green).

A schematic representation of the interactions, dotted lines for nonpolar contacts and red broken lines for hydrogen bonds, with the distances.

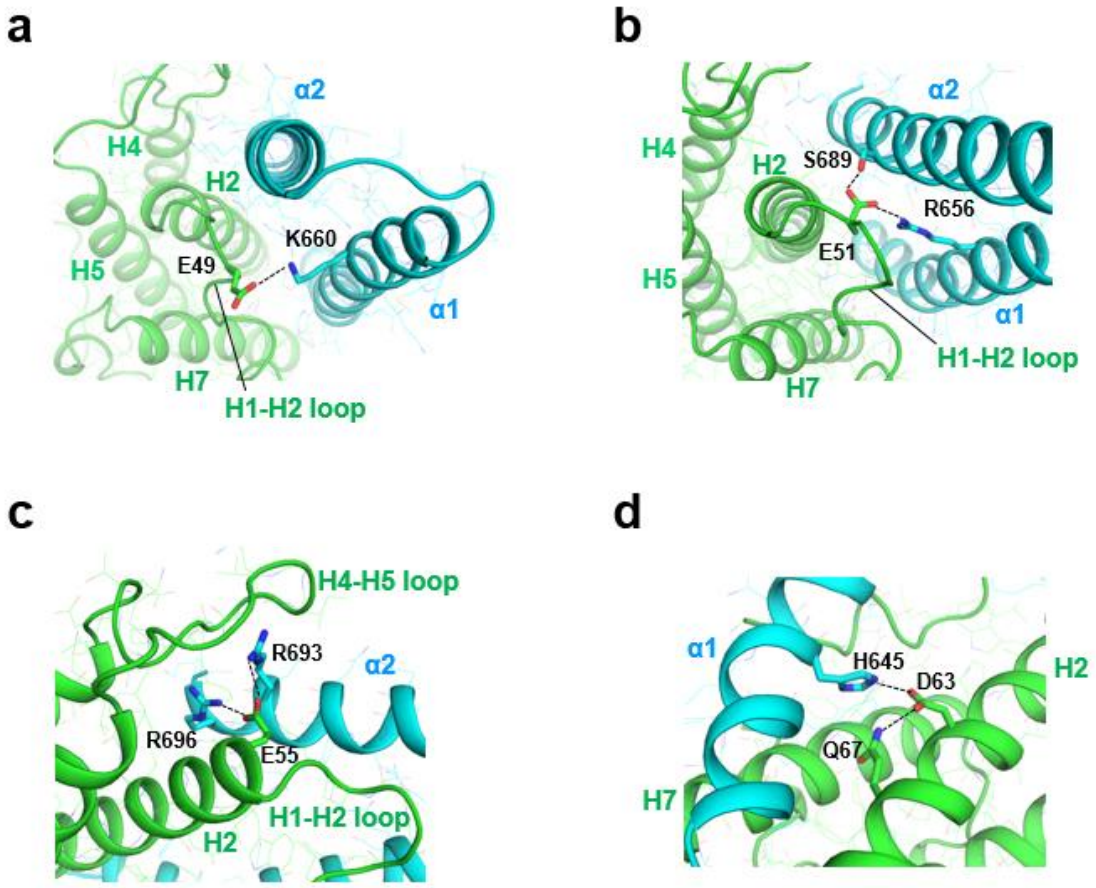

Figure 15. Salt bridging/hydrogen bonding interactions between the NTR domain of LATS1 and the negatively-charged nonpolar-patched surface of MOB1B.

(**a**) A close-up view of the intermolecular salt bridge/hydrogen bond with Glu49 (H1-H2 loop of MOB1B) and Lys660 (α1 helix of LATS1).

(**b**) A close-up view of the intermolecular salt bridge/hydrogen bond with Glu51 (MOB1B H1-H2 loop) and Arg656 (α1 helix of LATS1) and Ser6889 (α2 helix of LATS1).

(**c**) A close-up view of the intermolecular salt bridge/hydrogen bond with Glu55 (H2 helix of MOB1B) and Arg693 and Arg696 (α2 helix of LATS1).

(**d**) A close-up view of the intermolecular salt bridge/hydrogen bond with Asp63 (H2 helix of MOB1B) and His654 (α1 helix of LATS1), and Gln67 (MOB1B) stabilizing the Asp63 conformation.

Mutational analysis verified the interactions in MOB1B-LATS1 complex.

The observed MOB1B-LATS1 interactions in the structure were verified with mutational analysis. Alanine mutants of highly conserved arginine residues (R656A, R693A and R696A) displayed decreased binding affinity to less than 25% of the wild-type (**Fig. 16**). The S689E mutation, a phosphomimetic substitution, drastically decreased the affinity (to less than 20%). Mutation of both R659 and E688, which do not participate in direct interaction with MOB1B but stabilize the V-shaped structure by forming a salt bridge (**Fig. 13b**), resulted in a moderate reduction in the affinity (~50%). This implicates that the each NTR helices interact with MOB1 by complementary cooperated manner.

These mutational analyses are consistent with MOB1B-LATS1 complex structure and relevant experimental data from the literature, both with the *in vivo* and *in vitro* binding and kinase assays investigating mutations in human NDR1[27] and LATS1[29-30]. Thus, MOB1B-LATS1 complex structural data verify and significantly extend the reported structure of the pMOB1A-LATS1 complex [34].

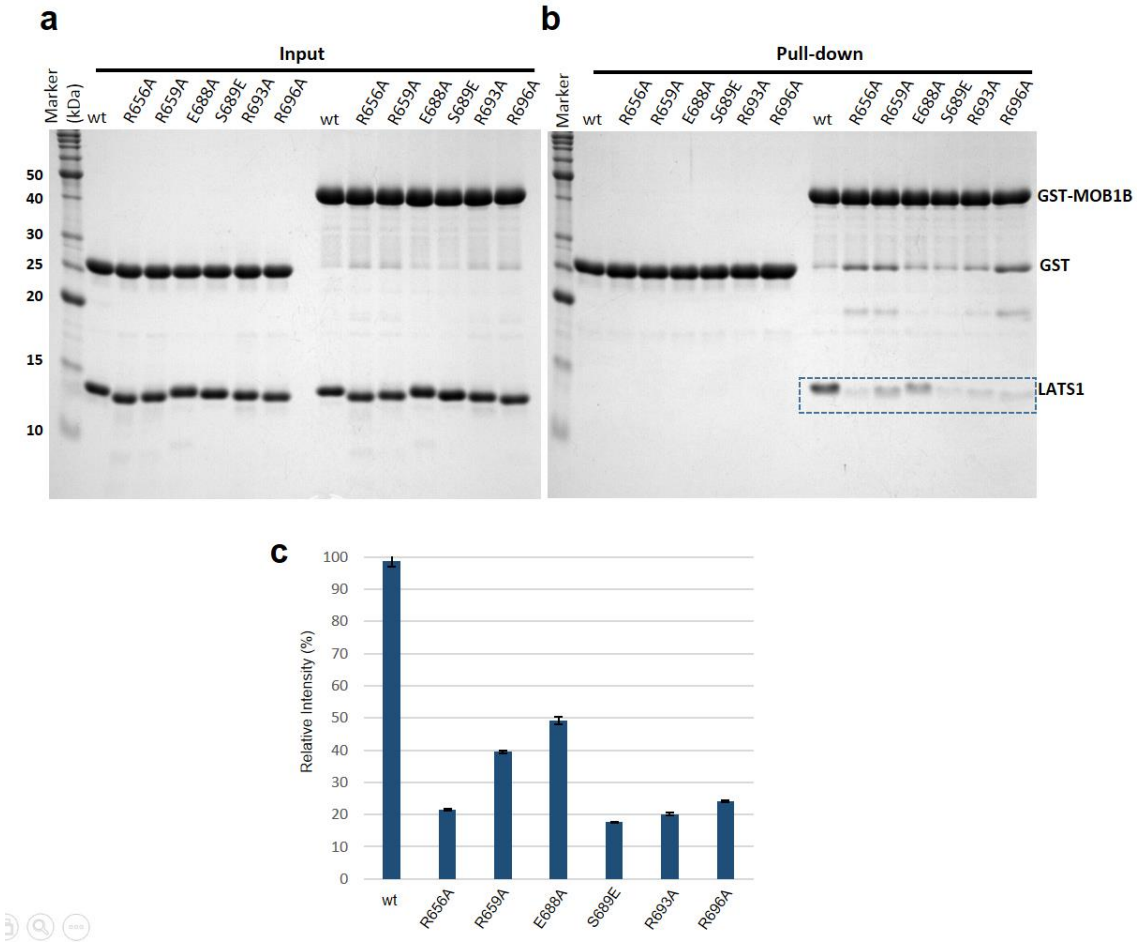

Figure 16. MOB1-LATS1 binding assay with mutations on the NTR domain of LATS1.

(**a**) Input of protein samples in pull-down binding assays of the wild and mutant NTR domains of LATS1 with GST-MOB1B of the N-truncated form (33-126).

(**b**) Pull-down binding assays of the wild and mutant NTR domains of LATS1 with GST-N-truncated MOB1B of the N-truncated form (33-126).

(**c**) Histogram of relative LATS1 binding to GST-MOB1B (33-126) (100% for the wild type) shown in **b**.

The MOB1 autoinhibition and the "pull-the-string" mechanisms of its relief inferred from a structural comparison between the autoinhibited and relieved forms

I compared the autoinhibited MOB1B structure with the recently reported structure of phosphorylated MOB1A in the pMOB1A-LATS1 complex[34] in an effort to define the structural changes induced by autoinhibition and its relief. The NTR domain of LATS1 forms a V-shaped bihelical structure comprising two long α-helices, αA and αB, and superposition of these structures shows direct overlap of the Switch helix with both αA and αB helices of the NTR domain (**Fig. 17a**), thus defining the conformational autoinhibition of MOB1 binding to LATS1 *via* the Switch helix of the N-terminal extension. No other segments of MOB1 display any direct interference in binding to the NTR domain.

The superimposed structures also show that the N-terminal extension residues (1-40) display a drastic conformational transition, whereas the H1 helix and following residues forming the core domain only undergo local conformational changes in the S2-H4 loop, which is partially disordered in both structures (**Fig. 17b**). The H1 helix of the autoinhibited form is followed by a sharp turn of Ser38-Gly39 and the Switch helix. The turn is stabilized by the Ser38 side chain forming hydrogen bonds with the main chains of Thr35 from the H1 helix and Asn40 from the Switch helix (**Fig. 10a**). This turn is absent in the phosphorylated form and the peptide chain is extended to run through the shallow groove formed by helices H6-H7 and H9 and is followed by a disordered region. The extended structure is stabilized by Ser38 interacting with the phosphate group of Thr35 and a short 3_{10}-helix (H0) formed by Leu-Leu-Lys at positions 28-30, which bind the hydrophobic site of the shallow groove. In the

autoinhibited form, the Leu-Leu-Lys segment is part of the Switch helix and two Leu residues participate in nonpolar interactions with the H2 helix.

The phosphorylated Thr12 residue of the pMOB1A-LATS1 complex is located close to the S2 strand so that the phosphate group is docked into the basic cluster pocket (**Fig. 17c**). The N-terminal end residues (1-9) are disordered but the three residues (13-15) that follow pThr12 form the S0 strand, which associates with the S2 strand to form a short antiparallel β-sheet. This S0-S2 β-sheet formation differs from that of the S_N-S2 β-sheet found in the autoinhibited form in several ways. First, the S_N strand of the autoinhibited form is formed by five residues and is longer than the S0 strand. Second, the residues forming the S_N strand are located at positions 5-9 (Phe5 to Ser9) and represent a 6-residue shift toward the N-terminal end (**Fig. 17d**). It is likely that on phosphorylation, the peptide chain of the N-terminal extension is pulled down toward the basic cluster pocket for phosphorylated Thr12 binding, resulting in a frame shift of residues forming the β-strand associated with the S2 strand. This shift should induce dissociation of the Switch helix, which is also accelerated by phosphorylation of Thr35 located at the helix. I refer to this mechanism as the "pull-the-string" mechanism for MOB1 activation.

The structure of the autoinhibited form of MOB1B showing the absence of large conformational changes in the MOB core domain suggests that truncation of the N-terminal extension converts the autoinhibited form to an active form. The N-terminal 32-residue truncated form (residue range 33-216), in which most of the Switch helix is removed, acts as an active form that binds the NTR domain of LATS1 (**Figs. 18a, b**). Phosphomimetic substitution of Thr12 and Thr35 with an aspartate residue also induces LATS1 binding. Intriguingly, the phosphomimetic forms exhibited stronger affinity than

the truncated form, implying that the phosphrylated N-terminal extension contributes to stabilization of the unmasked state. Indeed, a loop region between the H1 helix and the phosphorylated Thr35 residue contact the LATS1 NTR helix (**Fig. 17b**). The single phosphomimetic substitution of Thr12 activates LATS1 binding, and the double phosphomimetic substitution of both Thr12 and Thr35 induces further activation. Thus, phosphorylation of these two residues should cooperate to relieve autoinhibition by N-terminal extension.

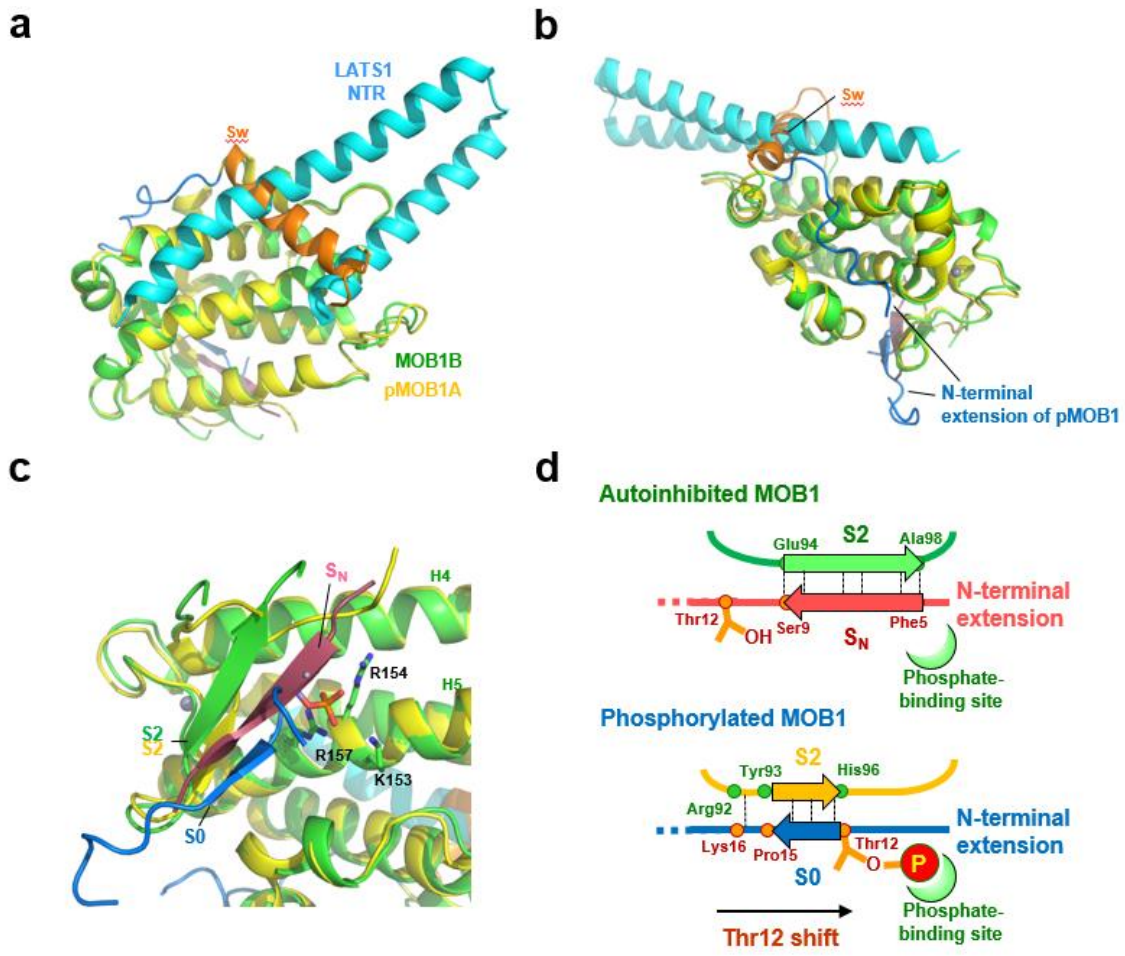

Figure 17. The structural autoinhibition of MOB1 inferred from structural comparison of full-length MOB1B with the pMOB1-LATS1 complex.

(**a**) Full-length MOB1B is superimposed on the phosphorylated MOB1A of the pMOB1A-LATS1 complex (PDB code 5BRK) with the overall r.m.s. deviation of 0.99 Å. The direct overlap of Switch helix of the full-length MOB1B and the NTR helices of LATS1 bound to phosphorylated MOB1A indicates that the autoinhibition is mediated by structural block of the LATS1-binding site by Switch helix.

(**b**) As in **a**, but the view to the backside from the LATS1-binding site to show the large conformational shifts of the N-terminal extension.

(**c**) A close-up view of overlay of the β-sheets formed by S0-S2-S1 strands of the full-length MOB1B and the phosphorylated MOB1A of the pMOB1A-LATS1 complex.

(**d**) A schematic drawing to show the shift of the N-terminal extension by phosphorylation. The phosphorylated Thr12 residue pull down the peptide chain of the N-terminal extension toward the backside of the MOB1 core domain to bind the phosphate-binding site.

Structural basis of MOB1 activation by binding to MST1/2

I compared the MOB1B autoinhibited structure with that of the N-truncated MOB1A bound to the phosphorylated MST2 peptide from a linker between the MST2 kinase and SARAH domains, hereafter referred to as the MOB1A-pMST2 complex[34] (**Fig. 18c**). The MST2 peptide has a phosphorylated threonine residue (pThr378) located at the N-terminal region, which forms a β1 strand associated with the S2 strand of MOB1A, with the phosphate group of pThr378 docked into the basic cluster pocket (**Fig. 18d**). This binding mode resembles that of the N-terminal extension of phosphorylated MOB1A, which forms a short β-sheet between the S0 and S2 strands with pThr12 docked into the basic cluster pocket (**Fig. 17c**). Furthermore, the β-sheet formed between the β1 strand of MST2 and the S2 strand of MOB1A is overlapped with the β-sheet of the S_N-S2 strands of autoinhibited MOB1B. This overlap induces competition between the β1 strand of MST2 and the S_N strand of autoinhibited MOB1, and should contribute to MOB1 activation by MST2 binding as previously observed[34]. In the MOB1A-pMST2 complex, the MST2 peptide forms a short α-helix (αA), which binds the hydrophobic sequence (HS)-binding site. Since this binding site is overlapped with the binding site for the H0 helix of the phosphorylated N-terminal extension in the pMOB1A-LATS1 complex, activation of MOB1 by binding to pMST2 *via* competition for binding to this overlapped binding site was proposed[34]. However, in MOB1B autoinhibited form, I did not observe binding of any region of the N-terminal extension to the HS-binding site.

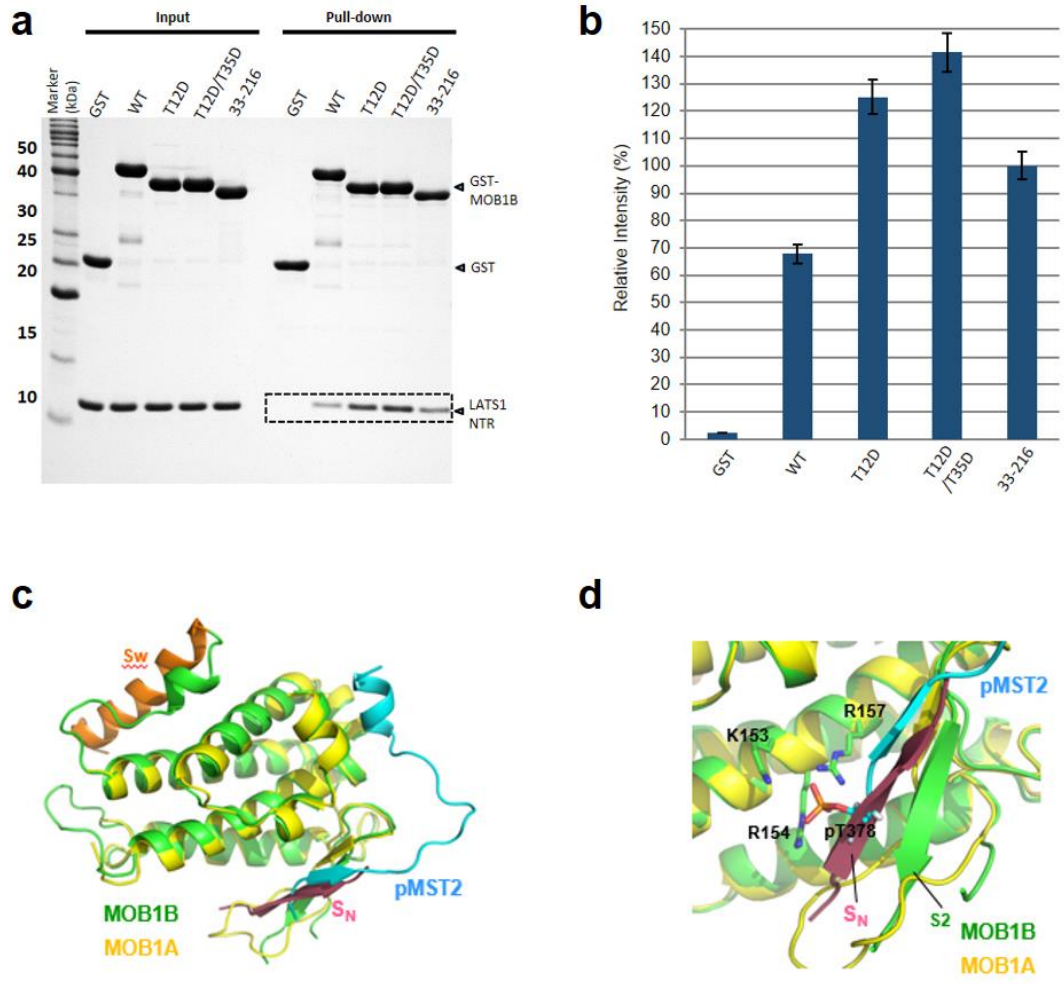

Figure 18. MOB1 autoinhibition by the N-terminal extension and its release by truncation or phosphorylation.

(a) Pull-down binding assays of the NTR domain of LATS1 with GST-MOB1B. MOB1B proteins are the N-terminal 32-residue truncated form (33-216), the wild type (WT) and double-mutant (T12/35D, phosphormimetic replacement of Thr12 and Thr35 with Asp) full-length forms.

(b) Histogram of LAT1 binding to GST-MOB1B shown in a.

(c) The full-length MOB1B superimposed on N-truncated MOB1A of the MOB1A-pMST2 complex (PDB code 5BRM). The backside from the LATS1-binding site is viewed to show the overlap of the SN strand of MOB1B and the β1 strand of pMST2. The hydrophobic sequence (HS) of pMST2 forms the short αA helix that binds helices H5, H6, H7 and H9 of MOB1. The MOB core domains are overlaid with an overall r.m.s. deviation of 0.87 Å.

(d) Close-up view of the overlay of β-sheets formed by the SN-S2 strands of full-length MOB1B and by the β1-S2 strands in the MOB1A-pMST2 complex. The phosphate group of pT378 of pMST2 binds the basic cluster pocket.

Comparison with the Mob2p-Cbk1p complex

A detailed comparison of MOB1B-LATS1 complex with the recently reported structure of the Mob2p-Cbk1p complexes was performed in detail [33] (**Fig. 19**). Superposition of the MOB1B and Mob2p structures showed fundamental similarity (r.m.s. deviaton of 1.45 Å), although a large local deviation was found in the H3-H4 loop conformation, which may have resulted from absence of two cysteine residues responsible for zinc ion coordination in Mob2p (**Fig. 7**). In stark contrast to the overall similarity of the MOB structures, the NTR domain of Cbk1p displays an unexpectedly different conformation from the bihelical V-shaped structure of the LATS1 NTR domain. The Cbk1p NTR domain forms a shorter α-helix, the αMOB helix, but lacks most of helical structures, including the α2 helix. Although the αMOB helix shows partial overlap with the N-terminal half of the LATS1 α1 helix, the residues assigned to this helix were shifted by 14 residues toward the C-terminus in the aligned sequences of the NTR domains (**Fig. 12c**, bottom). As a result of these differences, the Mob2p-Cbk1p interactions are completely distinct from those identified in the MOB1B-LATS1 and the pMOB1A-LATS1 complexes. I found that the Mob2p-Cbk1p interactions are inconsistent with relevant experimental data from the literature and my mutation studies. For example, Cbk1p residues (Ser337, Arg341 and Arg344) corresponding to conserved residues (Ser689, Arg693 and Arg696 of LATS1) participating in direct interactions with MOB1B, are located far from the MOB interface. Curiously, the peptide-chain tracing of the Cbk1p NTR domain roughly matches that of the LATS1 NTR domain, implying mis-tracing of the peptide chain of the Cbk1p NTR domain. I concluded that the structural discrepancies may not reflect any intrinsic differences between mouse MOB1B and yeast Mob2p structures, but rather are the result of

technical problems associated with the structure analyses of the Mob2p-Cbk1p complexes, probably due to poor electron density and resolution.

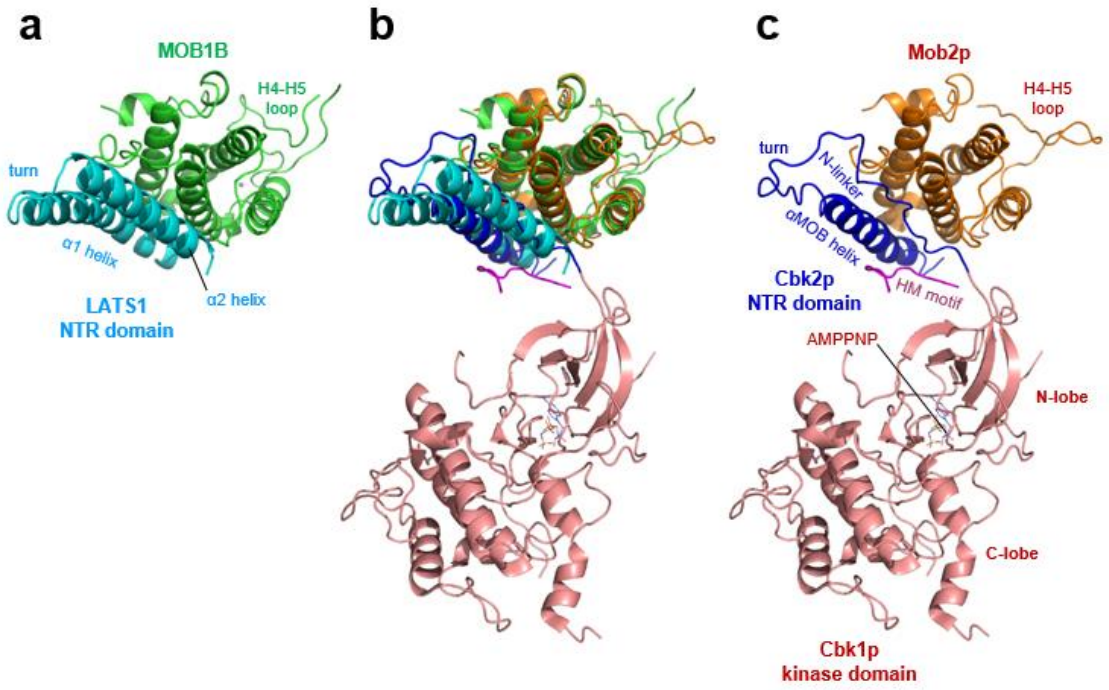

Figure 19. Structural comparison of the MOB1B-LATS1 complex and the Mob2p-Cbk1p complex.

(**a**) The MOB1B-LATS1 complex. The NTR domain (cyan) of LATS1 bound to MOB1B (green) is with labels for α1 helix, a turn and α2 helix.

(**b**) The superimposed structures shown in **a.** and **c**.

(**c**) The Mob1p-Cbk1p complex (PDB code 4LQS, at 3.3 Å resolution) ([33] Gogl, G. *et al*. 2015). The NTR domain (blue) of Cbk1p bound to Mob1p (orange) is consist of MOB1 helix, a turn and N-linker, which has no regular secondary structure. The kinase domain model lacks the N-lobe αC helix that is invisible in the map.

Structure of the N-truncated MOB1B and phospho-Sav1 complex

Hippo pathway is very similar with MEN of yeast in terms of phosphorylation cascade for regulation of cell division, except for occurring at the cytoplasmic membrane not at the spindle pole bodies. The reported Nud1(orthologue of Sav1)-like phospho-peptide and N-terminal truncated MOB1A complex structure gave me an inspiration which the phosphorylated Sav1 may directly interact with MOB1 even in the Hippo pathway. I explored the relevant region of the Nud1 phospho-peptide in the N-terminal Sav1 by similarity searching. Among the serine-threonine residues which are phosphorylated by MST2 in Sav1[53], I found that Ser36 in the region 29 LLRNLMP**S**FIRHGPT 43 will be the equivalent residue of Nud1 Thr78 (serine in the structure, **Fig. 20d**)[51]. Because the region shows a significant similarity with the MOB1-binding phospho-peptide of Nud1. I successfully crystallized and determined three-dimensional structure of the complex of N-terminal truncated MOB1B and the phospho-Sav1 peptide at 1.45Å resolution (**Figs. 20a, Table 4**). In the Sav1 phospho-peptide residues range of 34-41 structurally determined, the phospho-Ser36 is oriented exactly same position to the basic cluster pocket with the phospho- serine or threonine of previously reported structures (**Figs. 20b, c**) [34,51]. Residues Phe-Ile-Arg form a short antiparallel β-sheet which is equivalent with the Val-Val-Arg β-sheet of Nud1-like peptide (**Fig. 20d**). This structure strongly implicates MOB1 can make a complex directly with phosphorylated Sav1.

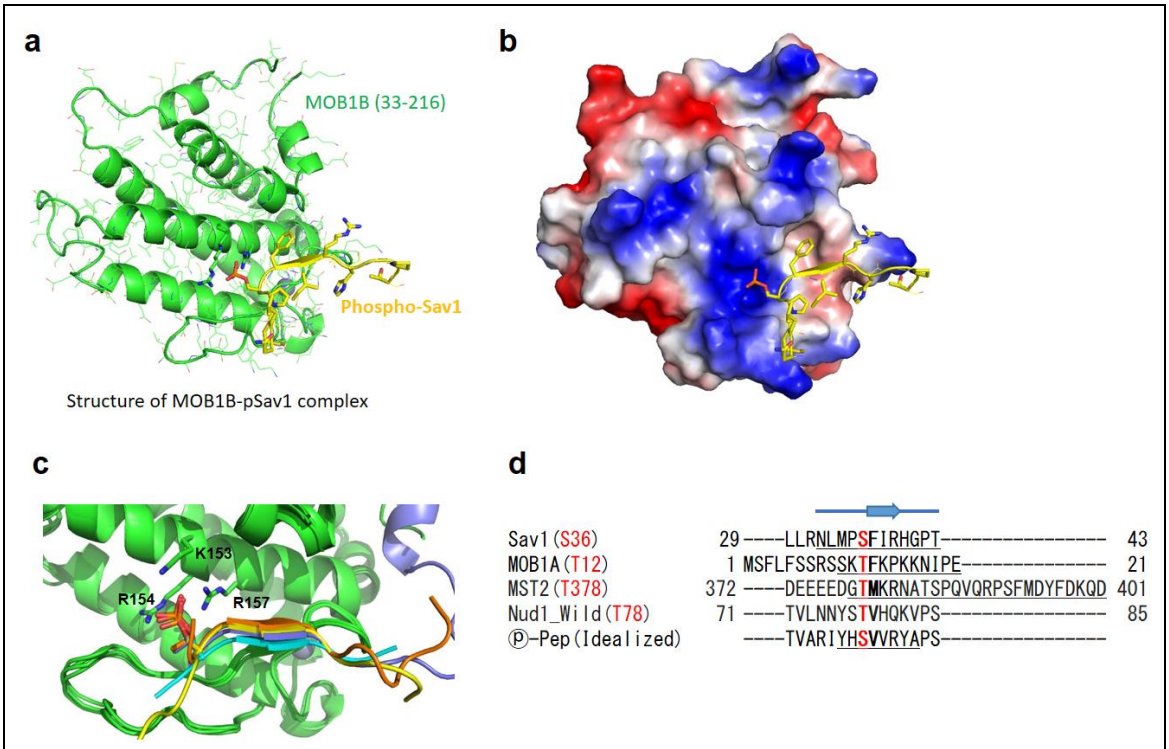

Figure 20. Structural comparison of the phospho-peptides interacting the basic cluster pocket.

(a) Structure of the complex between the N-truncated MOB1B (residues 33-216, green) and the phospho-sav1 (29-43, yellow) peptide.

(b) As in a, but MOB1B is shown as electrostatic potential surfaces and the phospho-sav1 in a ribbon model with side chains as in stick models.

(c)A close view of the basic cluster pocket region with superposition of the phospho-peptide and MOB1 complex models. MOB1 core domain is colored with green. MOB1A (orange, PDB code 5BRK), MST2 (Blue, PDB code 5BRM), Nud1-like (cyan, PDB code 4JIZ), and Sav1 (yellow) are depicted.

(d) Amino acid sequence alignment of the phospho-peptides. Structurally determined parts of each peptide are described as underlined. The phosphorylated Ser/Thr residues are colored in red.

Discussion

In the present study, I have elucidated the mechanism of MOB1 autoinhibition mediated by the N-terminal extension by structurally blocking the LATS1-binding site, and proposed that autoinhibition is relieved by phosphorylation which enhances dissociation of the N-terminal extension (**Fig. 21**). In the autoinhibited form of MOB1, the N-terminal extension forms the very N-terminal β-strand, the S_N strand (residues 5-9), forming a β-sheet with the S2 strand, followed by a conformationally flexible linker and the Switch helix bound to the LATS1-binding site. The flexible linker runs along the LATS1-binding surface with electrostatic interactions. Thr12 is located at the conformationally flexible linker and Thr35 is located at the Switch helix. The phosphorylation-mediated activation of MOB1 involves dissociation of the Switch helix, which is induced by steric effects following the phosphorylation of Thr35 and the binding of phosphorylated Thr12 and Thr35 to pT12 and pT35 binding pockets, respectively. The β-sheet between the S0 (residues 12-15) and S2 strands replaces that between the S_N and S2 strands. Interestingly, Thr35 is important in tissue specific processes as inferred from the tissue specific phosphorylation of Thr35[35].

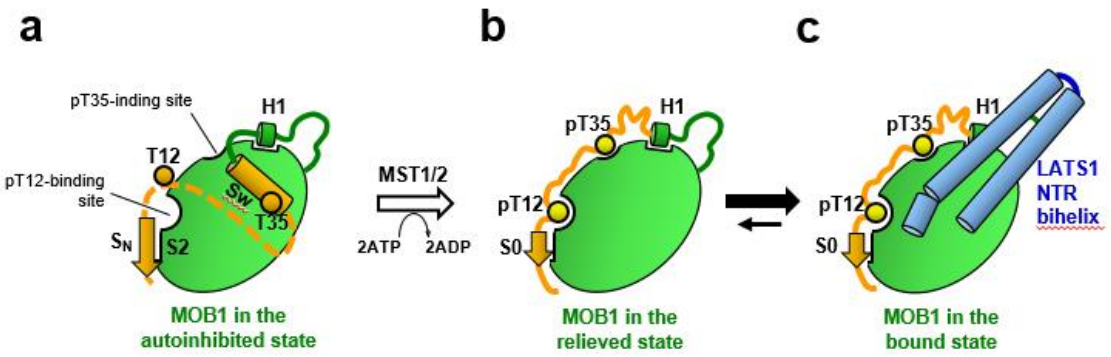

Figure 21. A model of autoinhibition and activation of MOB1.

(**a**) The autoinhibited form of MOB1. The N-terminal extension forms the very N-terminal β-strand, S_N strand (residues 5-9), forming a β-sheet with S2 strand, followed by a conformationally flexible linker (broken line) and Switch helix (Sw) bound to the LATS1-binding site. The linker between S_N strand and Switch helix may run at the LATS1-binding surface. Two key threonine residues, Thr12 and Thr35, are phosphorylated by MST1/2 on activation. Thr12 is located at the conformationally flexible linker but Thr35 is located at the Switch helix.
(**b**) The phosphorylation-medicated active form of MOB1. The autoinhibition is relieved by Switch helix unfolding, which is induced by steric effects of phosphorylation of Thr35 and bindings of phosphorylated Thr12 and Thr35 to pT12 and pT35 binding pockets, respectively. The β-sheet between S0 (residues 12-15) and S2 strands replaces that between.S_N and S2 strands. The LATS1 binding surface.
(**c**) The V-shaped α-helices of the NTR domain of LATS1 binds the LATS1 binding surface, of which autoinhibition is relieved by phosphorylation of the N-terminal extension that blocked the LATS1-binding surface of the MOB core domain.

Formation of the β-sheet between the S_N and S2 strands seems to be a key intramolecular interaction that contributes to the autoinhibition of LATS1 binding by the N-terminal extension. Phosphorylation of Thr12 by MST2 interferes with this interaction and results in formation of a β-sheet between the S0 and S2 strands by phosphate-binding to the basic residue cluster pocket. MOB1 is also activated by the phosphorylated peptide region of MST2, which forms a β-sheet with the S2 strand by competition with the S_N strand of autoinhibited MOB1[34]. This binding may play a role in formation of a ternary MST1-MOB1-LATS1 complex to accelerate phosphorylation of both MOB1 and LATS1, as previously suggested[34].

It is noticeable that the N-terminal 20 residues of MOB1 are highly positively charged with basic residues, one Arg and four Lys residues and no acidic residues. My

data suggested that this peptide region is conformationally flexible but critical for the MOB1 autoinhibition, probably mediated by electrostatic interaction with the negatively-charged LATS1-binding surface of MOB1. I speculate that formation of a β-sheet between the S_N and S2 strands contributes to autoinhibition by suppressing the conformationally dynamic properties of the flexible N-terminal extension, and stabilizes association of the N-terminal basic region to the negatively-charged LATS1-bindig surface of MOB1. These electrostatic interactions may stabilize association of the Switch helix with the LATS1-binding surface. This may account for the fact that removal of these basic residues by N-terminal truncation resulted in acceleration of LATS1 binding. I speculate that the S_N strand, the basic region and the Switch helix of MOB1 cooperatively contribute to autoinhibition by binding to each part of the MOB core domain.

Previous reports have suggested that Thr74 of MOB1 acts as a minor phosphorylation site[36,20]. In the structures, Thr74 is located at the C-terminal end of the H2 helix and in the MOB1B-LATS1 complex forms an intramolecular hydrogen bond with Glu175 (H7 helix), while its side-chain methyl group contacts the N-terminal end of the α1 helix of the NTR domain. The N-terminal flanking region of the α1 helix includes basic residues, electrostatic interactions of these residues with the phosphate group of Thr74 may possibly stabilize the MOB1B-LATS1 complex. In yeast, Mob1p is phosphorylated and regulated by the highly conserved Cdk1 kinase, whereas the major phosphorylation sites (Ser36 and Thr85) are located at the yeast-specific N-terminal extension[37], suggesting that this crosstalk might be specific to yeast cells.

Contrary to the importance of phosphorylation in MOB1 for binding to LATS/NDR

kinases, MOB2 does not possess conserved Thr12/Thr35 residues despite the high sequence homology of its core domain with MOB1 (**Fig. 7**). Moreover, MOB2 exhibits strong binding to NDR1/2 kinases but not to LATS1/2 kinases[30,32]. In the MOB1-LATS1 complex structure, four key Glu residues (at positions of 49, 51, 55 and 63 of MOB1B) required for direct interactions with LATS1 are not conserved in MOB2 proteins: Glu residues at positions of 49, 51 and 63 are replaced with Arg and Ile and Thr residues. These replacements could account, at least in part, for the failure of MOB2 to bind LATS1/2 kinases.

The binding of MOB2 to NDR kinases, however, could not be directly explained by an examination of MOB1B-LATS1 complex structure, due to the lack of key residues (Glu49, 51 and 63 of MOB1) required for direct interactions with LATS1 as mentioned above, whereas the binding of MOB1 to NDR kinases is well supported by the complex structure, which showed that key residues of LATS1 required for direct interactions with MOB1 are well conserved in NDR kinases (**Fig. 12c**). MOB2 binding to NDR1/2 kinases inactivates these kinases by blocking MOB1 binding necessary for stimulating phosphorylation of the A-loop and the hydrophobic motif[32]. I speculate that MOB2 binding to NDR kinases differs somewhat from that of MOB1 binding, even though the binding site of MOB2 is mostly or partly overlapped with that of MOB1. This hypothesis is supported by the NDR1 alanine mutations (Tyr31, Arg41, Arg44, Thr74 and Arg78), which had no effect on MOB2 binding but abolished MOB1 binding[32], since these NDR1 residues correspond to key LATS1 residues (Val646, Arg656, Arg659, Thr689 and Arg693, respectively) required for interactions with the NTR domain. Further structural studies, however, are needed to elucidate details of the MOB2 function.

In MOB1B-LATS1 complex structure, Ser689 of the LATS1 NTR domain is involved in direct interactions with MOB1B (**Figs. 14, 15b**) and the S689E mutation, a phosphomimetic substitution, almost abolished MOB1B binding (**Fig. 16**). However, the Ser689-equivalent residue of NDR1, Thr74, was reported as a putative phosphorylation site and phosphorylation is crucial for interaction with S100B[38]. On the other hand, the reported NMR structure of the S100B-NDR1 complex showed that Thr74 is not located at the S100B-NDR1 interface but is exposed to the solvent region[39]. Therefore, although the mechanism involving enhancement of S100B-NDR1 binding *via* Thr74 phosphorylation remains unknown, these results imply that activation of NDR kinases by S100B binding should differ from that involving MOB1.

Having understood the manner by which MOB1 can be regulated as a result of my study and previous structural work, another area that needs to be addressed is the manner by which MOB1 structurally regulates LATS/NDR kinase activities. MOB1 binding to NDR1/2 kinases triggers auto-phosphorylation of NDR1/2 on the A-loop, and also facilitates phosphorylation of the hydrophobic motif by MST kinases[27-28, 40-41,31-32]. In contrast, MOB1 binding to LATS1/2 kinases is only required for phosphorylation of the A-loop, while phosphorylation of the hydrophobic motif can be uncoupled from MOB1-LATS complex formation[19]. These facts suggest that LATS1/2 kinase activation by MOB1 should differ in some respect from that of NDR1/2 kinase activations, even though both are mediated by phosphorylation of the A-loop. The recently-reported structures of the Mob2p-Cbk1p complex showed that the NTR domain-bound Mob2p has no direct contact with the kinase catalytic domain, and is

located at some distance far from the A-loop at the active site[33] (**Fig. 19c**). Furthermore, the N-lobe displays a disordered structure, which lacks helices αB and αC, indicating that the structure should be that of an inactive form, as seen in the reported structure of Akt/PKB in the inactive OFF state[42]. Thus, the precise mechanism by which MOB1 accelerates A-loop phosphorylation remains unknown.

Phosphorylation dependent protein-protein interaction provides the foundation of many of signal transduction pathway. Four phosphorylated residues i.e. pSer36 of Sav1, pThr378 of MST, pThr of Nud1-like peptide, and pThr12 of intramolecular interaction of MOB1 interacting with the basic cluster pocket of MOB1 were structurally determined by this time (Fig. 8). I postulate these phosphorylation dependent interactions have a procedure. At first, as a scaffold protein Sav1 makes a complex with Merlin FERM domain at the plasma membrane in state of making complex with MST2[54]. Secondly, MST2 phosphorylates Sav1 to facilitate MOB1 retaining at the plasm membrane, and autophosphorylates its Thr378 residues for interacting MOB1 as a substrate. Thirdly, MST2 phosphorylates N-terminal residues Thr12 and Thr35 for making full active status of MOB1. Finally, MOB1 interacts with NTR domain of LATS to induce the LATS phosphorylation (**Fig. 22**).

The structure of MOB1B and phospho-Sav1 peptide complex give us a significant clue for the MOB1 membrane targeting mechanism. However, the interaction between Sav1 and MOB1 should be transient, because phospho-Ser36 of Sav1 is completely overlap with the phospho-Thr12 of MOB1. This intramolecular interaction is required for making the active status for interacting with LATS1 [34]. Therefore, MOB1 should be detached from the Merlin-Sav1-MST2 complex after recruiting at the plasm membrane.

Currently, there are no physiological evidences how this regulation can progress. Nevertheless, it is certain that this phosphorylation dependent assembly of Sav1 may have a pivotal role of MOB1 membrane targeting. Further research will be required for understanding this regulation mechanism.

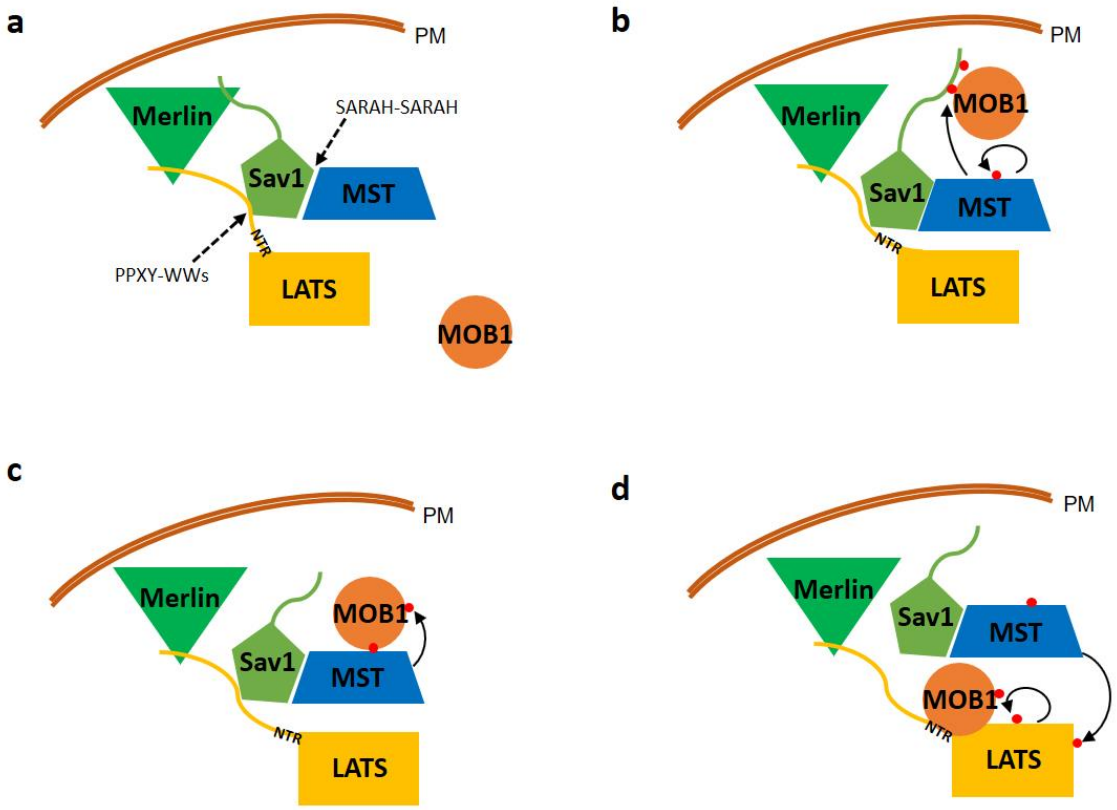

Figure 22. A model of phosphorylation dependent protein-protein interaction in the Hippo pathway.

(**a**) Merlin recruits LATS and MST-Sav1 complex at plasma membrane (PM). N-terminal conserved domain of LATS interact with merlin subdomain B. Meanwhile, N-terminal Sav1 binds to merlin subdomain C, which supports membrane retention of the MST-Sav1 complex.

(**b**) MST2 kinase phosphorylates N-terminal of Sav1. Phosphorylated Sav1 is released from merlin, then recruits MOB1 at the plasma membrane. Autophosphorylation of MST is required for interaction with MOB1 as an enzyme-substrate relationship.

(**c**) MST2 kinase phosphorylates MOB1. Phosphorylated MOB1 is fully activated form for LATS activation.

(**d**) The phosphorylated MOB1 binds to LATS NTR domain, which inducts both of the C-terminal phosphorylation by MST and the autophosphorylation in its A-loop.

In conclusion, my results have defined MOB1 autoinhibition involving the N-terminal extension containing the Switch helix, basic region and the S_N strand, and also revealed a “pull-the-string” mechanism by which Thr12/Thr35 phosphorylation activates MOB1. Additionally, the three-dimensional structure of phospho-Sav1 and MOB1 complex will give us a hint for understanding of the MOB1 membrane targeting mechanism.

These findings provide a physical basis for understanding the Hippo pathway, and a clue for the future development of inhibitor or activator compounds useful in the treatment of cancer by controlling the Hippo pathway *via* modification of LATS/NDR kinase activities.

Materials and methods

Cloning of MOB1B and LATS1 constructs.

The full-length cDNA clone of mouse MOB1B (GeneBank code NM026735) and LATS1 (GeneBank code BC158123) were purchased from Open Biosystems. The genes were subcloned into pGEX 6p-3 (GE healthcare) for N-terminal truncated MOB1B (residues 33-216), and pET49b (Merck) or pGEX 6p-3 for full-length MOB1B (1-216). The plasmids were transformed into *E. coli* strain BL21-CodonPlus RIL (Stratagene) or Rosetta2 (DE3) (Merck) for protein expression. Cloning regions of LATS1 were decided based on secondary structure prediction using the program Jpred 3[43]. DNA fragments of LATS1 (coding residues 604-703, and 621-703) were subcloned into pET47b (Merck) by polymerase chain reaction (PCR) amplification of the cDNA clone as a template. The fidelity of the coding region of all clones was confirmed by DNA sequencing.

Protein expression and purification.

MOB1B proteins were expressed in *E. coli* hosts which were grown in LB medium supplemented with antibiotics at 37°C to an OD_{600} of 0.6. Expression was induced by the addition of 100 μM isopropyl-β-D-thiogalactoside (IPTG) and 50 μM zinc acetate. Following incubation for another 20 hours at 18°C, cells were harvested by centrifugation. For the purification of full-length MOB1B, cells were suspended in 2× PBS (phosphate-buffered saline), containing 1 mM dithiothreitol (DTT), and then disrupted by sonication in an ice bath. The insoluble fraction was removed by

centrifugation and the supernatant was loaded onto a Glutathione Sepharose 4B affinity column (GE Healthcare). The column was washed with 3× PBS containing 1 mM DTT, and then the protein was collected using an elution buffer containing 20 mM Tris-HCl (pH 7.4), 0.1 M NaCl, 1 mM DTT and 20 mM glutathione. The column effluent containing GST-MOB1B was digested for 24 hours at 4°C with HRV 3C protease (Merck). The resultant product was loaded onto a HiTrap Q column (GE Healthcare) for GST-tag removal. The flow-through fractions were pooled and concentrated using Amicon Ultra centrifugal filter devices (10,000 MWCO, Millipore). Protein was finally purified through a Superdex 75pg gel filtration column (GE Healthcare) equilibrated with buffer (20 mM Tris-HCl (pH 7.5), 0.15M NaCl, and 1 mM DTT) (**Figs. 5a, b**). Protease inhibitors were not employed during the purification. Double-mutant (T12A/T35A) MOB1B was purified by the same procedure. N-terminal truncated MOB1B was also purified by the same procedure except that HiTrap Q column elution was effected using a 0.1 - 0.5 M NaCl gradient in buffer containing 25 mM Tris-HCl (pH 8.0) and 1 mM DTT (**Fig. 23c**).

For expression of the NTR domains (residues 604-703 and 621-703) of LATS1, plasmids were transformed into BL21 (DE3) Star™ (Invitrogen) which was grown in LB medium supplemented with antibiotics at 37°C to an OD_{600} of 0.6. Protein expression was induced by the addition of 500 μM of IPTG followed by incubation for another 4 hours at 38°C. Harvested cells were suspended in lysis buffer containing 20 mM Tris-HCl (pH 8.0), 0.5 M NaCl, 10 mM imidazole, and 3 mM β-mercaptoethanol, and then disrupted by sonication in an ice bath. Most of the LATS1 polypeptide was found in the insoluble fraction following centrifugation. For resolubilization of the polypeptide, the pellet was emulsified in PBS supplemented with 3 mM

β-mercaptoethanol, and then shaken vigorously for 12 hours at 42°C. The solubilized polypeptide was clarified by ultracentrifugation and the supernatant was loaded onto a Ni-NTA agarose affinity column (Qiagen). The column was washed with the lysis buffer, and protein was eluted using a buffer comprising 10 mM Tris-HCl (pH 8.0), 0.1 M NaCl, 3 mM β-mercaptoethanol, and 250 mM imidazole. Protein was further purified using HiTrap SP cation-exchange (GE Healthcare) and Superdex 75pg gel filtration columns. Protein purity was monitored during purification using polyacrylamide gel electrophoresis in the presence of sodium dodecyl sulfate (SDS-PAGE) (**Figs. 23a, b**).

Purified proteins were concentrated and their molecular weight confirmed by matrix-assisted laser desorption/ionization time-of-flight mass spectrometry (MALDI-TOF MS; Bruker Daltonics). Pull-down binding assays showed that both fragments specifically bound MOB1B.

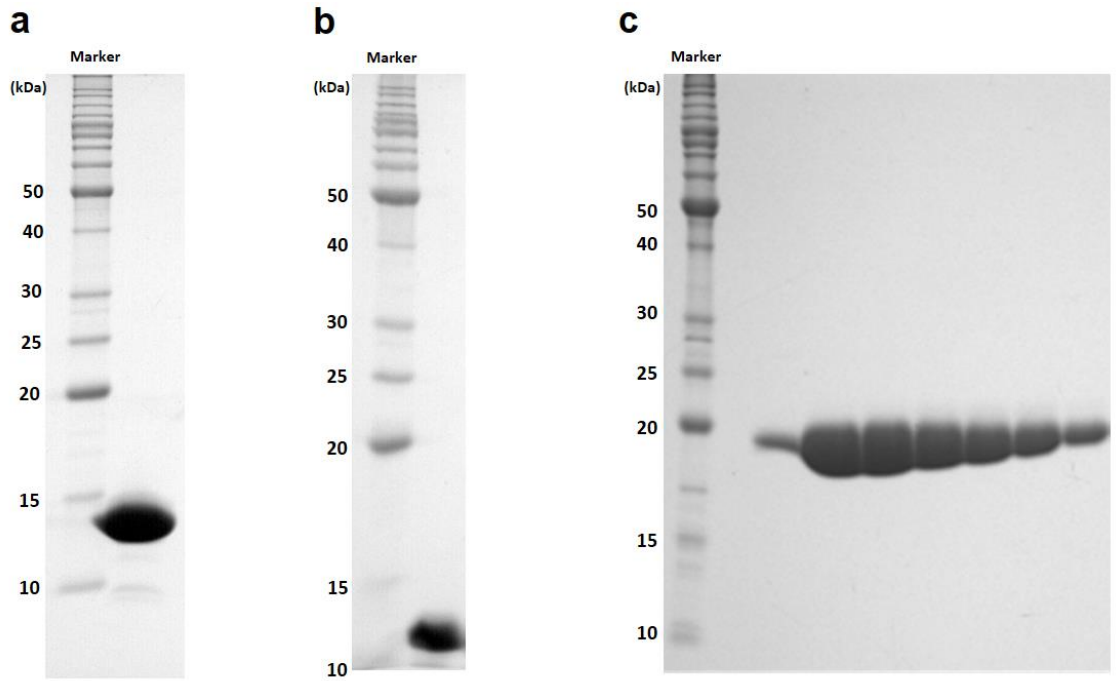

Figure 23. Purified LATS1 NTR domain constructs and N-truncated MOB1.

The purified proteins (a) LATS1 (residues 604-703), (b) LATS1 (residues 621-703), and MOB1B (residues 33-216) were analyzed by SDS-PAGE.

Crystallization and data collection.

Initial screening of the crystallization conditions was performed by the sitting-drop vapor diffusion method at 4°C and 20°C using Mosquito (TTP Labtech) and commercial crystallization kits (Qiagen JCSG I - IV, Sigma Crystallization kits, and Hampton Research Crystal Screen I, II, Index). Crystallization conditions were then optimized by the hanging drop vapor diffusion method with streak seeding to obtain single crystals suitable for X-ray diffraction. The optimized crystallization conditions for full-length MOB1B included a mixture of 1 μl protein solution (1.8 mM protein in the A buffer) and an equal volume of reservoir solution containing 10-13 % PEG 3350, 0.2 M ammonium fluoride, and 0.1 M MES (pH 6.5). Crystals were flash-frozen to 100 K in cryoprotectant solution containing 33-35 % (v/v) glycerol.

The best crystal of the MOB1B (33-216) and LATS1 (621-703) complex was obtained by mixing 1 μl protein solution (1.1 mM 1:1 molar ratio mixture in a stock buffer containing 10mM Tris-HCl (pH 7.5), 0.1M NaCl, and 0.25mM TCEP) and 1 μl reservoir solution containing 3-5 % PEG 4000 and 0.1 M Na-MES (pH 6.5). Crystals of the double-mutant T12D/T35D MOB1B (1-216) and LATS1 (621-703) complex were obtained by mixing 1 μl protein solution (0.8 mM 1:1 molar ratio mixture in a stock buffer containing 10mM Tris-HCl (pH 8.0), 0.1M NaCl, and 0.25mM TCEP) and 1 μl reservoir solution containing 20 % PEG 3350, 0.2 mM Sodium sulfate and 0.1 M MES

(pH 6.5).

The synthetic phospho-Sav1 peptide which the amino acid sequence is LLRNLMP(pS)FIRHGPT was purchased from Toray Research Center. The complex crystals of phospho-Sav1 and MOB1B (33-216) could be obtained in the condition mixing 1 μl protein solution (1.5-fold molar ratio of the synthetic peptide) and 1 μl reservoir solution containing 17-22 % PEG 3350, 0.2 M Na-Acetate and 0.1 M BisTris buffer (pH 6.3-7.3) at 4℃ and 20℃. Crystals in a cryo-protectant solution (reservoir solution containing 20% ethylene glycol) were flash-cooled in liquid nitrogen until use. I could obtain diamond-shaped crystals of full-length MOB1B, needle crystals of the MOB1B (33-216) and LATS1 (621-703) complex, and plate-shaped phopho-Sav1 peptide and MOB1B (33-216) crystals (**Fig. 24**).

X-ray diffraction data were collected on beamlines BL41XU and BL44XU at SPring-8, Japan, and then indexed and merged using the HKL2000 program suite[44]. Crystallographic data are summarized in Table 1, 2, 3 and 4.

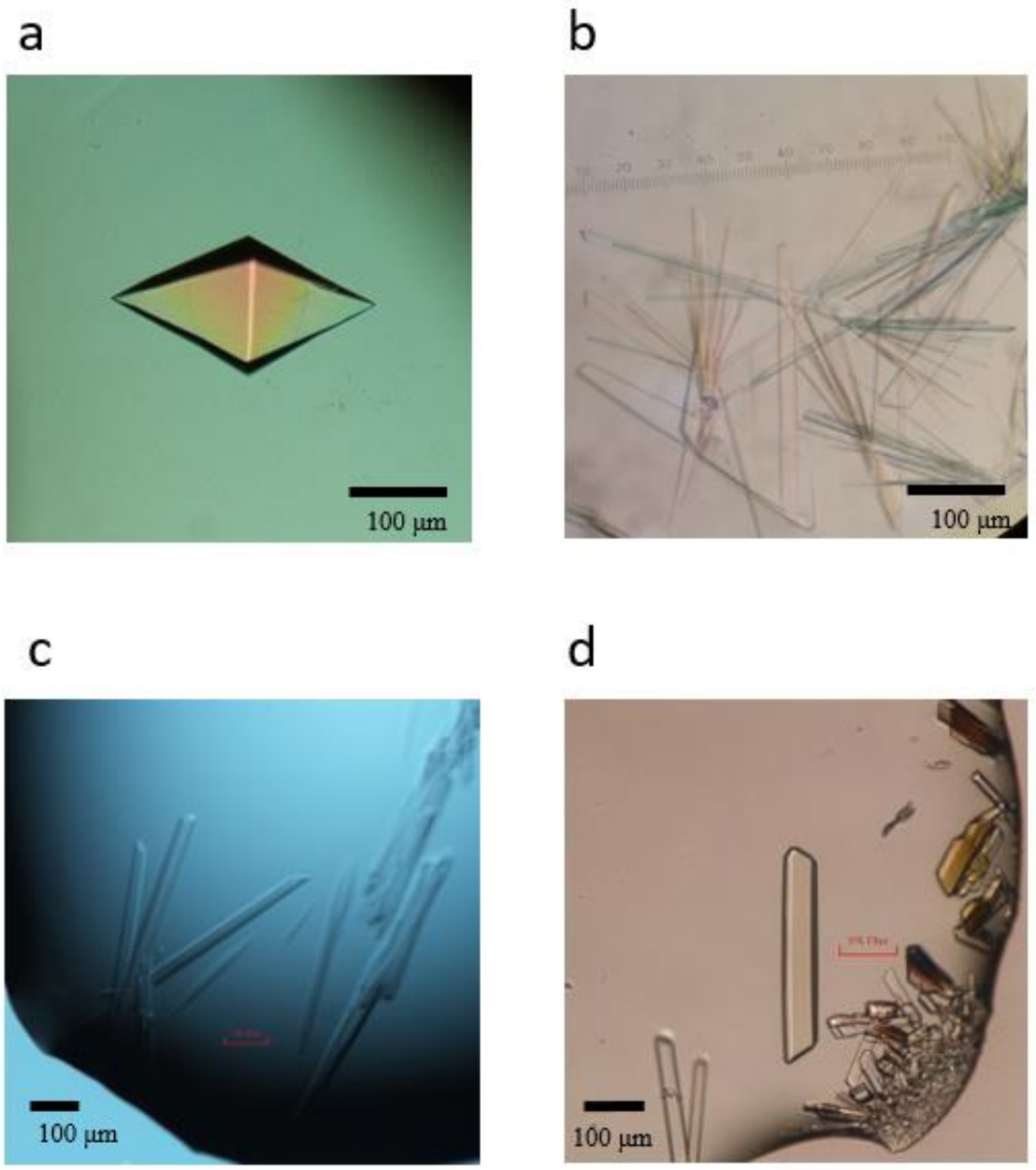

Figure 24. Crystals of full-length MOB1B, MOB1-LATS1 complex, MOB1(T12/35D)-LATS1 complex, and MOB1-pSav1 complex.

(**a**) A crystal of full-length MOB1B.

(**b**) Crystals of the complex between MOB1B (residues 33-216) and the LATS1 NTR (residues 621-703) domain.

(**c**) Crystals of the complex between MOB1B (T12/35D) and the LATS1 NTR (residues 621-703) domain.

(**d**) Crystals of the complex between MOB1B (33-216) and the phospho-Sav1 (residues 29-43) peptide.

Structure determination and refinement.

Phases of the MOB1B-LATS1 complex crystal structure were determined by molecular replacement using the program PHASER[45] with the model of MOB1A (PDB code 1PI1)[19] as a search model. An initial model equivalent to LATS1 was constructed using the PHENIX Autobuild program[46] and built manually with reference to the electron density map using Coot[47]. The model was refined using CNS[48] and PHENIX, and manual adjustments were made using Coot. The refined MOB1B (33-216) model was used as a molecular replacement (MR) for determining the phases of the full-length free MOB1B crystal structure. The initial model of the N-terminal region was built manually. Structural refinements were then performed by the same methods used for the complex. The crystal contains four crystallographically independent molecules A-D, whose structures are essentially the same (**Fig. 6b**). Two (molecules A and C) of the four molecules display a β-sheet between the S_N and S2 strands (see text). Using the refined MOB1B-LATS1 complex, the structure of the double-mutant MOB1B-LATS1 complex was determined and refined. The phase of the phospho-Sav1 and MOB1B (33-216) complex structure was also determined by MR with using the MOB1B (33-216) as a model. The structure of the phospho-Sav1 was built manually with reference to the electron density map using Coot. Superposition of the MOB molecules was performed using the program LSQKAB[49]. Illustrations were prepared using the program PyMOL (DeLano Scientific).

Preparation of mutant proteins and GST pull-down assays.

Mutant proteins were generated by PCR site-directed mutagenesis. PCR was performed using wild-type plasmids as a template, and the fidelity of the products was

confirmed by DNA sequencing. Mutant proteins were expressed using the same procedure employed for the wild-type. GST-MOB1B (wild-type and double-mutant T12D/T35D full-length forms) were purified using Glutathione Sepharose 4B affinity and HiTrap Q anion-exchange columns. LATS1 mutant polypeptides were resolubilized using the same method as described for the wild-type, and then subjected to further purification using Ni-NTA affinity and Superdex 75pg gel filtration columns. Purified proteins were concentrated, frozen in liquid nitrogen, and then kept at -80°C until use. To verify the MOB1B-LATS1 interactions, several point mutants of the NTR domain (621-703) were generated. However, I found that some of these mutants could not be utilized due to solubility issue. Therefore, the mutants of NTR domain (604-703) were used instead. The MOB1B-binding affinity did not differ between the two NTR constructs (**Fig. 25**). For the pull-down assay, GST-MOB1B (the N-terminal 32-residue truncated form) and LATS1 proteins (40 μM) were mixed in 1:1 molar ratio in 200 μl assay buffer containing 20 mM Tris-HCl (pH 7.5), 0.3 M NaCl and 1 mM DTT, and then applied to 100 μl Glutathione Sepharose 4B resin equilibrated with the same buffer. The resin was washed three times with 700 μl assay buffer and centrifugation (500 g for 5 min) at 4 °C, followed by verification of the supernatant OD_{280} at a basal level. Resin-attached proteins were then eluted using 150 μl assay buffer supplemented with 30 mM glutathione, and the effluents analyzed by 15% SDS-PAGE. Band intensities were visualized using LAS-4000 (Fujifilm), and quantitative analyses were performed using the program ImageGauge (Fujifilm).

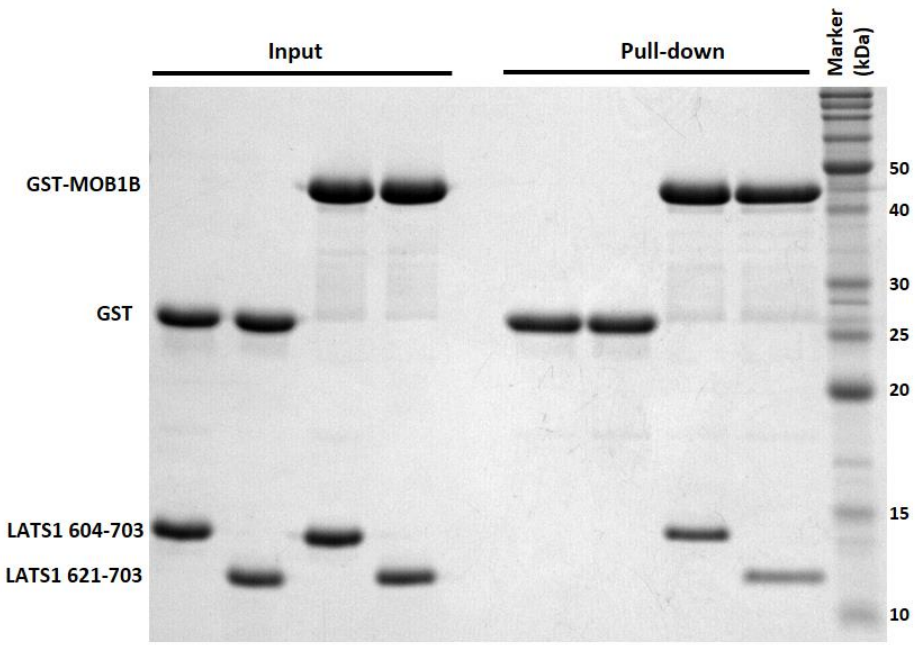

Figure 25. The NTR domain constructs used for the GST pull-down assay show same affinity with GST-MOB1B (33-216)

Analytical ultracentrifugation (AUC).

Sedimentation velocity ultracentrifugation experiments were performed at 20 °C using a Beckman Coulter Optima XLA analytical ultracentrifuge equipped with an An-60 Ti rotor and double-sector centerpieces as previously described[50]. Protein samples adjusted to 19 μM in buffer containing 20 mM Tris-HCl (pH 7.5) and 0.1M NaCl were centrifuged at 20,000 rpm (32,198 g) and then scanned at a wavelength of 280 nm. Radial absorbance scans were measured 99 times every 12 minutes at a wavelength of 280 nm. For high protein concentration analysis, MOB1B adjusted to 200 μM in the same buffer was scanned at 300nm for saturation issue. The resultant data were analyzed using the program SEDFIT.

References

1. Edgar, B.A. From cell structure to transcription: Hippo forges a new path. *Cell* **124**, 267-73 (2006).
2. Saucedo, L.J. & Edgar, B.A. Filling out the Hippo pathway. *Nat Rev Mol Cell Biol* **8**, 613-21 (2007).
3. Zhao, B., Tumaneng, K. & Guan, K.L. The Hippo pathway in organ size control, tissue regeneration and stem cell self-renewal. *Nat Cell Biol* **13**, 877-83 (2011).
4. Ramos, A. & Camargo, F.D. The Hippo signaling pathway and stem cell biology. *Trends Cell Biol* **22**, 339-46 (2012).
5. Harvey, K.F., Zhang, X. & Thomas, D.M. The Hippo pathway and human cancer. *Nat Rev Cancer* **13**, 246-57 (2013).
6. Johnson, R. & Halder, G. The two faces of Hippo: targeting the Hippo pathway for regenerative medicine and cancer treatment. *Nat Rev Drug Discov* **13**, 63-79 (2014).
7. Huse, M. & Kuriyan, J. The conformational plasticity of protein kinases. *Cell* **109**, 275-82 (2002).
8. Yin, F. *et al*. Spatial Organization of Hippo Signaling at the Plasma Membrane Mediated by the Tumor Suppressor Merlin/NF2. *Cell* **154**, 1342-1355 (2013).
9. Lignitto, L. *et al*. Proteolysis of MOB1 by the ubiquitin ligase praja2 attenuates Hippo signalling and supports glioblastoma growth. *Nature Communications* **4**(2013).
10. Kim, M. *et al*. cAMP/PKA signalling reinforces the LATS-YAP pathway to fully suppress YAP in response to actin cytoskeletal changes. *Embo Journal* **32**,

1543-1555 (2013).

11. Serrano, I., McDonald, P.C., Lock, F., Muller, W.J. & Dedhar, S. Inactivation of the Hippo tumour suppressor pathway by integrin-linked kinase. *Nat Commun* **4**, 2976 (2013).
12. Bae, S.J. *et al*. NEDD4 controls intestinal stem cell homeostasis by regulating the Hippo signalling pathway. *Nat Commun* **6**, 6314 (2015).
13. Luca, F.C. & Winey, M. MOB1, an essential yeast gene required for completion of mitosis and maintenance of ploidy. *Mol Biol Cell* **9**, 29-46 (1998).
14. Mah, A.S., Jang, J. & Deshaies, R.J. Protein kinase Cdc15 activates the Dbf2-Mob1 kinase complex. *Proc Natl Acad Sci U S A* **98**, 7325-30 (2001).
15. Wei, X., Shimizu, T. & Lai, Z.C. Mob as tumor suppressor is activated by Hippo kinase for growth inhibition in Drosophila. *Embo Journal* **26**, 1772-1781 (2007).
16. Hergovich, A., Stegert, M.R., Schmitz, D. & Hemmings, B.A. NDR kinases regulate essential cell processes from yeast to humans. *Nat Rev Mol Cell Biol* **7**, 253-64 (2006).
17. Nelson, B. *et al*. RAM: A conserved signaling network that regulates Ace2p transcriptional activity and polarized morphogenesis. *Molecular Biology of the Cell* **14**, 3782-3803 (2003).
18. Jansen, J.M., Barry, M.F., Yoo, C.K. & Weiss, E.L. Phosphoregulation of Cbk1 is critical for RAM network control of transcription and morphogenesis. *Journal of Cell Biology* **175**, 755-766 (2006).
19. Praskova, M., Xia, F. & Avruch, J. MOBKL1A/MOBKL1B phosphorylation by MST1 and MST2 inhibits cell proliferation. *Curr Biol* **18**, 311-21 (2008).
20. Bao, Y. *et al*. Roles of mammalian sterile 20-like kinase 2-dependent

phosphorylations of Mps one binder 1B in the activation of nuclear Dbf2-related kinases. *Genes Cells* **14**, 1369-81 (2009).

21. Stavridi, E.S. *et al.* Crystal structure of a human Mob1 protein: toward understanding Mob-regulated cell cycle pathways. *Structure* **11**, 1163-70 (2003).
22. Ponchon, L., Dumas, C., Kajava, A.V., Fesquet, D. & Padilla, A. NMR solution structure of Mob1, a mitotic exit network protein and its interaction with an NDR kinase peptide. *J Mol Biol* **337**, 167-82 (2004).
23. Mrkobrada, S., Boucher, L., Ceccarelli, D.F., Tyers, M. & Sicheri, F. Structural and functional analysis of *Saccharomyces cerevisiae* Mob1. *J Mol Biol* **362**, 430-40 (2006).
24. Rock, J.M. *et al*. Activation of the yeast Hippo pathway by phosphorylation-dependent assembly of signaling complexes. *Science* **340**, 871-5 (2013).
25. Chung, H.Y., Gu, M., Buehler, E., MacDonald, M.R. & Rice, C.M. Seed sequence-matched controls reveal limitations of small interfering RNA knockdown in functional and structural studies of hepatitis C virus NS5A-MOBKL1B interaction. *J Virol* **88**, 11022-33 (2014).
26. Zhou, D. *et al*. Mst1 and Mst2 maintain hepatocyte quiescence and suppress hepatocellular carcinoma development through inactivation of the Yap1 oncogene. *Cancer Cell* **16**, 425-38 (2009).
27. Bichsel, S.J., Tamaskovic, R., Stegert, M.R. & Hemmings, B.A. Mechanism of activation of NDR (nuclear Dbf2-related) protein kinase by the hMOB1 protein. *J Biol Chem* **279**, 35228-35 (2004).
28. Hergovich, A., Bichsel, S.J. & Hemmings, B.A. Human NDR kinases are rapidly

activated by MOB proteins through recruitment to the plasma membrane and phosphorylation. *Mol Cell Biol* **25**, 8259-72 (2005).

29. Bothos, J., Tuttle, R.L., Ottey, M., Luca, F.C. & Halazonetis, T.D. Human LATS1 is a mitotic exit network kinase. *Cancer Research* **65**, 6568-6575 (2005).
30. Hergovich, A., Schmitz, D. & Hemmings, B.A. The human tumour suppressor LATS1 is activated by human MOB1 at the membrane. *Biochemical and Biophysical Research Communications* **345**, 50-58 (2006).
31. Hergovich, A. *et al.* The MST1 and hMOB1 tumor suppressors control human centrosome duplication by regulating NDR kinase phosphorylation. *Curr Biol* **19**, 1692-702 (2009).
32. Kohler, R.S., Schmitz, D., Cornils, H., Hemmings, B.A. & Hergovich, A. Differential NDR/LATS interactions with the human MOB family reveal a negative role for human MOB2 in the regulation of human NDR kinases. *Mol Cell Biol* **30**, 4507-20 (2010).
33. Gogl, G. *et al*. The Structure of an NDR/LATS Kinase-Mob Complex Reveals a Novel Kinase-Coactivator System and Substrate Docking Mechanism. *PLoS Biol* **13**, e1002146 (2015).
34. Ni L, Zheng Y, Hara M, Pan D, Luo X. Structural basis for Mob1-dependent activation of the core Mst-Lats kinase cascade in Hippo signaling. *Genes Dev*. **29**, 1416-1431 (2015).
35. Huttlin, E.L. *et al*. A tissue-specific atlas of mouse protein phosphorylation and expression. *Cell* **143**, 1174-89 (2010).
36. Hirabayashi, S. *et al*. Threonine 74 of MOB1 is a putative key phosphorylation site by MST2 to form the scaffold to activate nuclear Dbf2-related kinase 1. *Oncogene*

27, 4281-4292 (2008).

37. König, C., Maekawa, H. & Schiebel, E. Mutual regulation of cyclin-dependent kinase and the mitotic exit network. *J Cell Biol* **188**, 351-68 (2010).
38. Tamaskovic, R., Bichsel, S.J., Rogniaux, H., Stegert, M.R. & Hemmings, B.A. Mechanism of Ca2+-mediated regulation of NDR protein kinase through autophosphorylation and phosphorylation by an upstream kinase. *Journal of Biological Chemistry* **278**, 6710-6718 (2003).
39. Bhattacharya, S., Large, E., Heizmann, C.W., Hemmings, B. & Chazin, W.J. Structure of the Ca2+/S100B/NDR kinase peptide complex: Insights into S100 target specificity and activation of the kinase. *Biochemistry* **42**, 14416-14426 (2003).
40. Stegert, M.R., Hergovich, A., Tamaskovic, R., Bichsel, S.J. & Hemmings, B.A. Regulation of NDR protein kinase by hydrophobic motif phosphorylation mediated by the mammalian Ste20-like kinase MST3. *Mol Cell Biol* **25**, 11019-29 (2005).
41. Vichalkovski, A. et al. NDR kinase is activated by RASSF1A/MST1 in response to Fas receptor stimulation and promotes apoptosis. *Curr Biol* **18**, 1889-95 (2008).
42. Yang, J. *et al.* Crystal structure of an activated Akt/protein kinase B ternary complex with GSK3-peptide and AMP-PNP. *Nat Struct Biol* **9**, 940-4 (2002).
43. Cole, C., Barber, J.D. & Barton, G.J. The Jpred 3 secondary structure prediction server. *Nucleic Acids Res* **36**, W197-201 (2008).
44. Otwinowski, Z. & Minor, W. Processing of X-ray diffraction data collected in oscillation mode. *Macromolecular Crystallography, Pt A* **276**, 307-326 (1997).
45. Mccoy, A.J. *et al*. Phaser crystallographic software. *Journal of Applied Crystallography* **40**, 658-674 (2007).

46. Adams, P.D. *et al*. PHENIX: a comprehensive Python-based system for macromolecular structure solution. *Acta Crystallogr D Biol Crystallogr* **66**, 213-21 (2010).

47. Emsley, P. & Cowtan, K. Coot: model-building tools for molecular graphics. *Acta Crystallogr D Biol Crystallogr* **60**, 2126-32 (2004).

48. Brunger, A.T. *et al*. Crystallography & NMR system: A new software suite for macromolecular structure determination. *Acta Crystallogr D Biol Crystallogr* **54**, 905-21 (1998).

49. Kabsch, W. Solution for Best Rotation to Relate 2 Sets of Vectors. *Acta Crystallographica Section A* **32**, 922-923 (1976).

50. Mori, T., Gotoh, S., Shirakawa, M. & Hakoshima, T. Structural basis of DDB1-and-Cullin 4-associated Factor 1 (DCAF1) recognition by merlin/NF2 and its implication in tumorigenesis by CD44-mediated inhibition of merlin suppression of DCAF1 function. *Genes Cells* **19**, 603-19 (2014).

51. Jeremy M. Rock, et al. Activation of the Yeast Hippo Pathway by Phosphorylation-Dependent Assembly of Signaling Complexes. *Cell* 340, 871-875 (2013)

52. Li-Lun Ho, et al. Mob as tumor suppressor is activated at the cell membrane to control tissue growth and organ size in *Drosophila*. *Dev. Biol.* 337, 274-283 (2010)

53. Byoung Hee Park & Yong Hee Lee Phosphorylation of SAV1 by mammalian ste20-like kinase promotes cell death. *BMB reports* **44**(9), 584-589 (2011).

54. Jianzhong Yu, et al. Kibra Functions as a Tumor Suppressor Protein that Regulates Hippo Signaling in Conjunction with Merlin and Expanded. *Dev. Cell.* **18**, 288–299, (2010)

55. Manning, G., Whyte, D. B., Martinez, R., Hunter, T. & Sudarsanam, S. The protein kinase complement of the human genome. Science 298, 1912-1934, doi:10.1126/science.1075762 (2002).

56. A. Hergovich, MOB control: Reviewing a conserved family of kinase regulators *Cellular Signalling* **23** 1433–1440 (2011)

Acknowledgments

I deeply appreciate to my supervisor, professor T. Hakoshima. I would like to express my best gratitude to him for his guidance and discussion throughout all my works.

I would like to specially thank to Dr. K. Kitano for lots of practical advices for crystallographic studies.

I gratefully acknowledge a favor to Dr. T. Mori and Dr. Y. Hirano for their many advisements.

I cannot forget saying thanks to Ms. Y. Tachioka for her supporting this study.

I would like to show my deep sense of gratitude to Ms. M. Shirakawa for her supporting DNA works.

Finally, I wish to thank colleagues, all members of our laboratory for their supporting and discussing about my works.